UNIVERSITY OF CALIFORNIA,
IRVINE

An Analytical Evaluation of Passive-Resistance Performance of Highway Bridge Abutment Walls Using Incrementally Mobilized Shear Stresses

THESIS

submitted in partial satisfaction of the requirements
for the degree of

MASTER OF SCIENCE

in Civil Engineering

by

James David Maximilian Collett

Thesis Committee:
Associate Professor Anne Lemnitzer, Chair
Assistant Professor Mo Li
Professor Ricardo Andrés Moffat Covarrubias

2018

DEDICATION

To

my wife Samantha

who tolerates so much from me

and

to every engineering student

that thinks there must be a better way

Better a patient person than a warrior,

one with self-control than one who takes a city

Proverbs 16:32 (NIV)

TABLE OF CONTENTS

LIST OF FIGURES

LIST OF TABLES

LIST OF VARIABLES

Some papers referenced herein may vary in their symbolic nomenclature.

a	Failure plane angle or Coulomb wall angle (θ)
β	Backfill slope angle (θ)
c'	Effective cohesion (F/A)
c'_m	Mobilized eff.cohesion (F/A)
γ'	Effective unit weight (F/V)
d	Depth (L)
δ	Wall Interface Friction (angle)
Δ *or* y	Wall horizontal deflection (L)
Δx	Width of soil slice (L)
ε_a	Axial strain (% or dec.)
h	Wall height (L)
I_B	Influence factor (unitless)
K	Earth pressure coefficient or stiffness (unitless or F/L or F/L^2)
K_0	At-rest earth pressure coefficient
K_{50}	Stiffness at 50% of ultimate wall passive capacity (F/L or F/L^2)
K_a	Active earth pressure coefficient
K_p	Passive earth pressure coefficient
L	Wall length (L)
M	Inverse of soil compression modulus (A/F)
OCR	Overconsiolidation Ratio
P	Resultant force (F or F/L)
P_a	Active resultant force (F or F/L)
P_p	Passive resultant force (F or F/L)
ϕ'	Effectve friction angle (θ)
ϕ'_m	Mobilized eff. Friction angle (θ)
PSD	Principal stress difference (F/A)
R	Radius (L)
R_0	Initial log-spiral radius (L)
Rf	Reduction Factor
σ'_0	At-rest effective horizontal earth pressure (F/A)
σ'_1	Major principal effective stress (F/A)
σ'_3	Minor principal effective stress (F/A)
σ'_a	Active earth pressure (F/A)
σ'_p	Passive earth pressure (F/A)
σ'_v	Vertical effective stress
X	Horizontal distance (L)

ACKNOWLEDGMENTS

I thank my committee chair, Professor Anne Lemnitzer, for challenging me and teaching me that research is as much about the process as it is the result. She is a role model to her students and peers as not only a brilliant researcher and great success in her field, but also as an intentional, kind human being. I would be remiss in not also thanking her and her husband, Carter, for encouraging my wife and me as we set up our lives and careers.

I thank my committee member, Professor Ricardo Moffatt, for the idea that began this journey, for his intellect and expertise, and for his constructive insights and advice. He was an indispensable sounding board as I worked through the concepts presented herein.

I thank my committee member, Professor Mo Li, for her willingness to engage and participate in the shaping of this thesis. It takes a brave, brilliant scholar to willingly jump into the tedious world of geotechnics. I am grateful that she did so on my behalf.

I thank Patrick Wilson, doctoral graduate from the University of California, San Diego and esteemed member of the Southern California geotechnical community, for sharing detailed experimental test data, that saved dozens of hours of digitizing and back-calculating.

I thank my boss, Daniel Dufrenne, for his mentorship, time, and flexibility. Dan went above and beyond any obligation as an employer to make sure I had the time and resources to prioritize my education for the past five years.

Lastly, I thank my family, specifically my wife, Samantha, for her love, patience, and support; my parents, for setting me up for success and teaching me the value of integrity; my grandparents, for supporting me and taking an interest in my work; my in-laws, for

rooting for me in everything I set out to accomplish; and my grand-uncle, Robert Gregory, who invested many hours of time and energy to make sure I had the tools to succeed in the world of higher education.

ABSTRACT OF THE THESIS

An Analytical Evaluation of Passive-Resistance Performance of Highway Bridge Abutment Walls Using Incrementally Mobilized Shear Stresses

By

James David Maximilian Collett

Master of Science in Civil Engineering

University of California, Irvine, 2018

Professor Anne Lemnitzer, Chair

Abutment walls are integral components of bridge superstructures and play an important role in resisting lateral forces due to static and dynamic loading. Empirical methods for calculating lateral passive earth pressures are desirable computational tools in the design of bridge abutment systems. This thesis examines the development of lateral pressures behind a simple, vertical bridge abutment by analyzing the development of engineering strains in the fill material upon lateral loading. Laboratory testing, such as triaxial shear strength testing was conducted and/or evaluated on fill soils implemented in three unique load tests published in literature. The stress-strain curves from these tests were analyzed with respect to normal stresses and shear strains, and used to develop a mobilized shear strength profile for each representative soil type. Using log-spiral passive wedge failure modeling as proposed by Terzaghi combined with recent lateral displacement models found in literature, peak passive resistance was predicted within 17% of the experimental results with all case studies, with the load-deflection curve shape in general agreement with the measured curve for both strong and brittle wall failures.

1 INTRODUCTION

At its heart, the study of geotechnical engineering consists of a universe of methods and resources for predicting, analyzing, and utilizing the strength performance of soil in the construction of a variety of structures, ranging from fill slopes to skyscrapers. These methods seek to account for the variety of soil materials and material properties, specifically relating to the varying magnitudes of strength anisotropy. Where most prevalent empirical methods have fallen short is in providing meaningful behavior analysis with respect to strains. The calculation of earth pressures—such as for retaining wall design—specifically reflects this shortcoming, with the most common forms of analysis consisting of static limit equilibrium analysis methods like that developed by Rankine, and highly approximated assumptions of strains required to develop various earth pressure cases. Computer-based modeling solutions using finite element or finite difference analysis, like FLAC (ITASCA, 2018) or PLAXIS (Brinkgreve, 2014), are capable of modeling displacement-based behavior of retained soil, but are both often cumbersome for anything but large scale design projects, and only provide the framework to do such analysis, relying on the user to program detailed soil strength profiles. Duncan and Mokwa (2001) and Shamsabadi, et al. (2005, 2008, 2012) provide empirical methods to estimate the passive earth pressure development with respect to strain, but rely primarily on fitting parameters with limited account for the more dilatant shear behavior seen in highly compacted soils.

This research work seeks to overcome some of the currently known limitations by developing a simple methodology for the estimation of passive earth pressures using strain

measurements from laboratory triaxial testing. This approach accounts for the incrementally mobilized strength behavior in soils and is applicable to loosely and densely compacted backfill materials. The method may be executed with a simple math-based computer script, or a slightly more complex Excel spreadsheet.

2 BACKGROUND

Undoubtedly as long as humankind has been building, it has been conceiving methods by which to move and retain earth. The quintessential solution to the problem of creating a vertical elevation change between two earth surfaces is the retaining wall, a structure whose purpose is to maintain the stability of what would otherwise be a vertical or near-vertical excavation into a slope or elevated area. Figure 2.1 shows a typical concrete and masonry retaining wall under construction, which was used to cut into the ascending slope, increasing the lower level area.

Figure 2.1: A cantilever retaining wall constructed of concrete masonry units (CMU) and Portland Cement Concrete (PCC)

The retaining wall has, in some form or fashion, become a common feature of construction of all kinds, ranging from providing a barrier around a medieval fortress to extending a homeowner's backyard further out over a slope. Given their prevalence and utility, it should be no surprise that early attempts at understanding the mechanics of

retaining walls formed the foundations of geotechnics. Charles-Augustin de Coulomb, the noted physicist, first published his theory on lateral earth pressures acting on retaining walls in 1776; his method is still prevalently used to this day. While there are a variety of types and uses of retaining walls, some of which are discussed below, all require a similar understanding of the lateral earth forces as a part of the design process, wherein earth pressures are weighed both as driving (active/at-rest) and resisting (passive) loads against the capacities, geometry, and properties of the given retaining wall. Figure 2.2 illustrates various common types of retaining walls, which are discussed in detail below.

Types of Retaining Walls

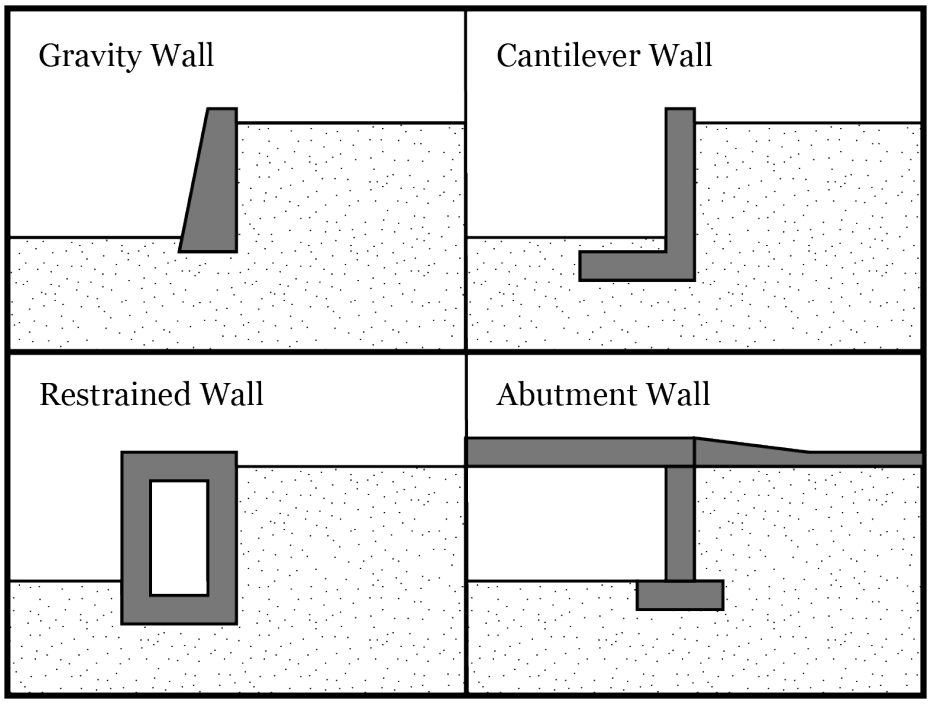

Figure 2.2: General sections of various types of retaining walls

Gravity walls

The simplest of retaining structures, mechanically speaking, is the gravity wall, which relies on its self-weight to contain and restrain the backfill soil. For a gravity wall to be stable, it must be able to resist sliding, bearing failure, and overturning, corresponding to force equilibrium in the horizontal and vertical directions, as well as moment equilibrium in the projected third dimension, respectively. As such, geometry, scale, and weight are key components for the overall stability of the wall, often resulting in heavy structures with a relatively large footprint. Gravity walls may consist of native or man-made materials, and may either be monolithic or segmented structures. Highway abutment walls are often constructed as gravity walls, specifically if they only rest on the abutment seat foundation for bearing support, and do not receive rigid resistance against sliding or overturning from the seat.

Cantilever Walls

Like gravity walls and most other wall systems, cantilever walls rely on retention and redistribution of forces to satisfy force and moment equilibriums. However, rather than using a large mass to retain earth, cantilever walls implement a more slender profile. A wall footing is designed to provide bearing support, sliding resistance, and a resisting moment which connects to a vertical stem that performs the actual retention of the soil (cantilevering out from the foundation). Cantilever retaining walls may employ shallow or deep foundation systems, and may be constructed using different types of materials, though the most common configurations are often constructed as reinforced concrete and concrete masonry structures. Specialty wall systems that are commonly associated with

cantilever retaining walls include pile-based shoring, such as sheet piles, secant piles, and soldier piles with lagging.

Restrained-Type Walls

When a retaining wall system is braced and prevented from deflecting in any significant way, the retained soil is unable to relax, and thus imparts additional pressure upon the wall. This configuration is called a restrained wall; a further discussion of lateral earth pressure development may be found below. Restrained walls are common, and may or may not also be classified as gravity or (very rigid) cantilever walls. Most common restrained retaining wall types include braced shoring systems, basement walls, and some variations of tieback walls.

Other Retaining Wall Types

Other wall types include, among others, Mechanically Stabilized Earth (MSE) walls, which use geotextiles (synthetic meshes) lain horizontally in designed spacing to disrupt any potential plane of instability and embed deeper into the wall backfill. Given that this retention system allows some level of backfill deformation/relaxation, active pressure conditions are usually developed and assumed, with the analysis consisting of equilibrium evaluation between the driving force of the retained soil and the pull-out and breaking resistance of the geotextile material.

Figure 2.3: A typical overpass abutment wall (The Reinforced Earth Company 2014)

Figure 2.3 shows a typical highway overpass abutment wall, which support overpass bridges where roadways intersect, allowing traffic to pass in orthogonal directions simultaneously. These abutments usually consist of thick, reinforced concrete blocks that both support the overpass bridge and retain soil backfill. Given the impetus of transportation research in contemporary engineering, abutment walls have been a primary focus of study with regard to earth pressures and displacement-based performance.

Design Overview

A typical retaining wall design process constitutes of (1) the quantification of stresses and other specific characterizations to the earth to surround the retaining wall; (2) the design of the retaining wall to resist global loads applied to the wall by the earth, primarily by iterating the geometry, size, and embedment of the wall; and (3) the design of the retaining wall to resist internal or localized stresses, namely through specification of wall materials and thicknesses, reinforcement quantities and locations, etc. The final product of a successful design process is a wall that is stable against any potential combination of applied forces --for example, pressures resulting from the statically retained fill material, wind loading on the abutment face, impact loading from vehicular or vessel traffic, surcharge loading on the backfill (e.g., street traffic), or potential earthquake forces. These various loading cases are compared to resisting strengths that are reduced by factors of safety, so that the ultimate strength of the geostructural system is never exceeded. This approach is known as *allowable stress design* (ASD). An alternative design method, the *Load Resistance Factored Design* (LRFD) approach, applies individual modification factors to both loads and resisting strengths by increasing the applied loading and reducing the available capacity. While the ASD method is still commonly used in engineering practice, the *LRFD* methodology is gaining increasing traction as various codes and design manuals adopt it as a preferred design method. Given that retaining walls are designed to conform to equilibrium of forces and moments with respect to *factored* strengths, the ability to quantify both the magnitudes and behaviors of both loads and resisting strengths is crucial to the design and analysis processes.

Understanding Lateral Earth Pressures

Lateral earth pressure have traditionally, and most commonly, been described in relation to the corresponding vertical earth pressures, due to the fact that, like most structural mediums, soil transmits stresses from one orthogonal direction to another. However, since soil is an inelastic material, unique relationships are developed to correlate stresses in varying directions under different boundary and loading conditions. The lateral earth pressure coefficient, *K*, represents the relationship between horizontal and vertical effective soil stresses, in accordance with Equation 2.1:

$$K = \frac{\sigma'_h}{\sigma'_v} \tag{2.1}$$

In essence, the lateral earth pressure coefficient is the ratio of horizontal earth pressure to vertical earth pressure at any given point. Since vertical earth pressure is dependent on overburden loading and surcharges, lateral earth pressure is linearly dependent of the same pressure contributions. Lateral earth pressures are generally understood and analyzed within three different cases which form solution envelopes: at-rest conditions, active conditions, and passive conditions. While this document focuses primarily on the analysis of passive conditions in retaining walls, the other cases are briefly summarized. Figure 2.4 illustrated the generalized differences in scale magnitudes between active and passive pressures with respect to vertical pressure. For most cases earth pressure distributions are approximated triangularly as shown in Figure 2.4, even though in some instances, and specifically with regard to braced shoring or restrained walls in clay soils, distributions may be assumed trapezoidal or as other geometric shapes.

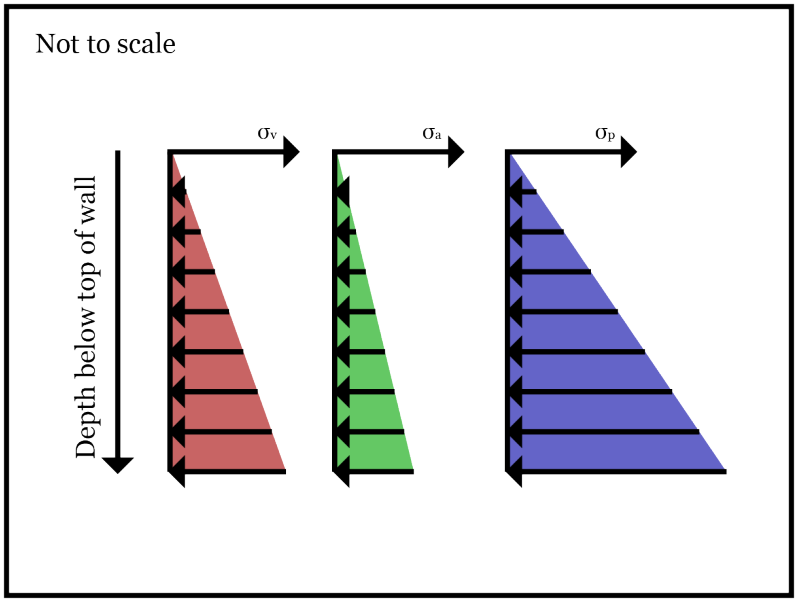

Figure 2.4: Generalized depiction of vertical, active, and passive pressures over depth

At-Rest Lateral Pressure

The at-rest or static lateral earth pressure considers the development of horizontal pressures in a soil mass that is confined and restrained from mobilization. This scenario applies to the case of a backfill wedge behind a very rigid retaining wall, or pressure against a cast-in-place drilled shaft foundation. While undergoing rigid confinement, no slip plane develops in the soil, and therefore the mobilization of any resisting shear strength in the soil is prevented. At-rest lateral earth pressures are commonly represented with the pressure coefficient K_0. Jaky (1948) proposed equation 2.2 to predict at-rest lateral pressures as a function of vertical stresses, where K_0 varies as a function of the soil friction angle.

$$K_0 = 1 - \sin(\varphi') \tag{2.2}$$

This equation was later expanded by Mayne and Kulhawy (1982) as equation 2.3, introducing an additional dependence on the overconsolidation ratio (OCR) of the soil (which can be extended to account for specialized loading cases, the effects of compaction effort, etc.).

$$K_{0(NC)} = [1 - \sin(\varphi')] * OCR^{\sin(\varphi')} \quad (2.3)$$

While these equations provide reasonable estimates of pressures that are otherwise difficult to evaluate in-situ, they are entirely empirical, and do not provide any explanation or theory behind earth pressure propagation.

Active Earth Pressure

If a vertical cut or retained soil wedge is not rigidly confined and a slip plane is allowed to develop, shear stresses will develop along that mobilized surface to oppose the slippage of the soil mass. These shear stresses work in resistance to the laterally transmitted stresses, lowering the lateral earth pressure from the at-rest pressure to the *active* pressure. The most common methods of solving for the active earth pressure were provided by Coulomb (1776) and Rankine (1857), which are discussed in part later as a component of the literature review. While precise methods for evaluating active earth pressures as a function of displacement are not readily available, the mobilization required to develop the active case is commonly evaluated in relationship to the strength nature of the subject soil, with brittle soils (clays, silts) developing active-level pressures with much

less mobilization than stronger, more granular soils (sands, gravels). Figure 2.5 illustrates the typical development of active earth pressure in the backfill of a retaining wall.

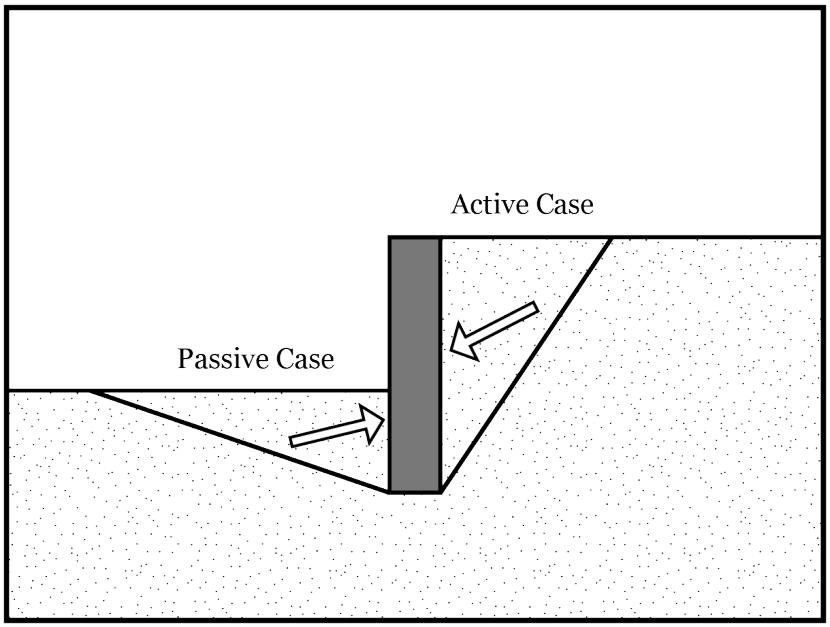

Figure 2.5: Development of active and passive resistance in a retaining wall. Arrows illustrate forces imparted on the wall by the soil wedges.

Passive Earth Pressure:

While active pressure conditions create driving stresses in the soil towards the retaining structure and seek to displace the retaining element away from the backfill soil,, the *passive* soil pressure condition mobilizes a resisting force inside a retained soil to prevent the lateral movement of a retaining wall into the backfill soil, as shown in Figure 2.5. In this case, lateral pressure increases from the at-rest condition as resistance develops along the weakest slip plane in the soil. Similarly to the active condition, the two most common methods for evaluating the passive resistance of a given soil structure are the

procedures proposed by Coulomb (1776) and Rankine (1857), which are related in theory and execution to the respective active case equations.

In addition, the development of passive resistance requires some mobilization of the soil, which is the central concept of this research and analysis. Figure 2.6 shows the generalized relationship between retaining wall mobilization (into backfill for the passive case, and away from the backfill for the active case) and lateral earth pressure development. While displacement tolerances are often built into the design of retaining walls to allow for the development of active or passive pressures, the values used are taken primarily from generalized soil properties, rather than soil-specific load-displacement behavior data, which has historically been difficult to incorporate into design work.

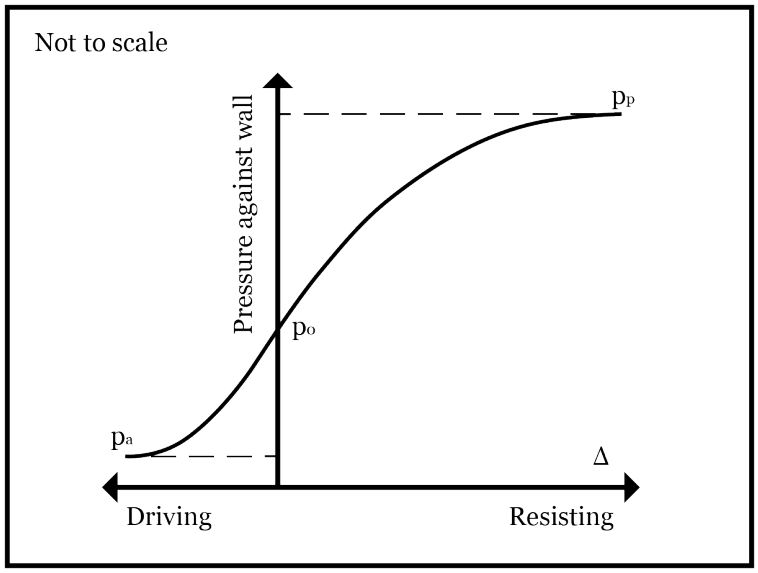

Figure 2.6: Lateral earth pressure relationship to lateral wall deflection

Assuming non-cohesive soil and a triangular pressure distribution, earth pressures and resultant forces are evaluated according to the following equations, with component forces (horizontal, vertical, etc.) and resultants evaluated geometrically:

$$\sigma'_h = K * \sigma'_v = K * \gamma' * h \tag{2.4}$$

$$P_h = \frac{1}{2} * K * \gamma' * h^2 \tag{2.5}$$

3 LITERATURE REVIEW

Classical Solutions for Passive Earth Pressures

Coulomb (1776)

The first comprehensive attempt to analyze the development of earth pressures behind retaining walls was made by Charles-Augustin Coulomb, the renown French scientist and engineer. Coulomb (1776) suggested that lateral strengths against vertical structures against level earth gradients could be analyzed via trial wedge optimization, wherein multiple linear failure plane geometries are attempted via limit equilibrium calculations, and the resultant of the critical failure wedge (i.e. the wedge formed by the shear plane of least resistance) is determined to be the solution. Coulomb's work was later expanded by Mayniel (1808) and Muller-Breslau (1906) to account for the effects of friction between the retaining wall and the immediately adjacent soil, as well as for sloped backfills and battered walls (walls not perpendicular to the horizon). The modern Coulomb formula is shown as Equation 3.1, with variables as previously defined, and illustrated in Figure 3.1:

$$K_p = \frac{cos^2(\varphi+\theta)}{cos^2\theta\,\cos(\delta-\theta)*\left(1-\sqrt{\frac{\sin(\delta+\varphi)\sin(\varphi+\beta)}{\cos(\delta-\theta)\cos(\beta-\theta)}}\right)^2} \tag{3.1}$$

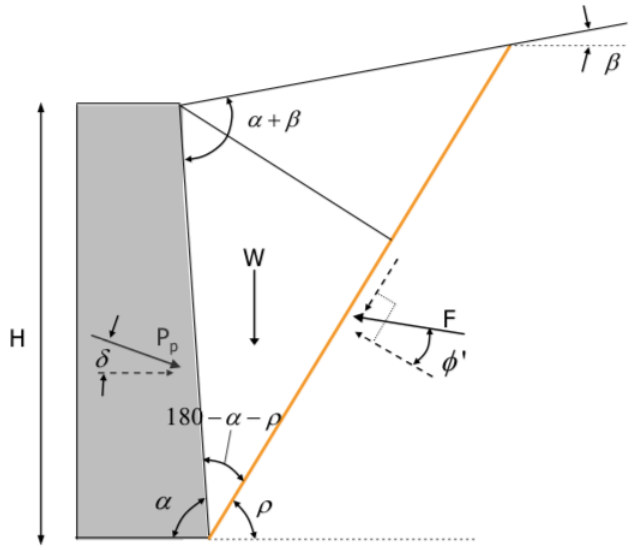

Figure 3.1: Sliding block passive case model as used by Coulomb method (Lemnitzer 2007)

Notable in Coulomb's theory is the use of limit equilibrium conditions and the use of trial optimization. His approach formed a pattern that would be repeated in several successively published methods. Under limit equilibrium conditions, ultimate material strengths are used to analyze the conditions and configuration by which that material fails under stress (Chen 1968). Given an additional assumption that the material undergoing stress is both relatively rigid and plastic, one might infer that a clearly defined failure plane may be determined. In this case, forces along the failure plane may be analyzed, as opposed to the analysis of a stress field over the entire section of interest, thus creating a block analysis scenario. While soil is in fact not perfectly plastic, nor immune to significant levels of creep, the use of limit equilibrium block methods has, in the centuries since Coulomb's publication, become one of the most prevalent means of analyzing soil structures where residual strengths are of interest, specifically within the realms of retaining wall analysis,

slope stability, and seismic design; largely due to the simplicity and typical conservatism of the analysis.

Rankine (1857)

Rankine (1857) proposed an analytical solution to active and passive earth pressures, based on the assumption that soil exhibits perfectly plastic, incompressible behavior. Ignoring cohesion (as did Coulomb, initially), Rankine's method evaluates the backfill failure plane as the plane that first reaches the peak tensile capacity of the material, initially taking into account level backfill conditions against a plumb wall surface (no batter). When reduced to its simplest form, the earth pressure coefficient for passive conditions is evaluated as Equation 3.2, with the angle of the resulting failure plane evaluated as Equation 3.3 in relation to the horizontal, taken from the heel of the retaining structure. When accounting for sloped backfill conditions, Rankine's method is represented by the more complex Equation 3.4, where α in this case refers to the slide plane angle:

$$K_P = \tan^2(45° + \frac{\varphi'}{2}) \tag{3.2}$$

$$\alpha = 45° - \frac{\varphi'}{2} \tag{3.3}$$

$$K_P = \frac{\cos(\beta)+\sqrt{(cos^2\beta - cos^2\varphi)}}{\cos(\beta)-\sqrt{(cos^2\beta - cos^2\beta)}} * \cos(\beta) \tag{3.4}$$

Despite its convenience, there are several shortfalls implicit in Rankine's assumptions that preclude its accuracy or universality. First, the method fails to account for any impact on lateral earth pressure due to wall-soil shear resistance (i.e. interface

friction), which all other methods discussed herein take into account. Hence the Rankine solution yields pressure estimates with lower (passive case) or higher (active case) magnitudes than Coulomb, Terzaghi and other methodologies. In general however, the assumption to neglect interface friction places Rankine lateral earth pressure solutions as conservative in comparison to other prevalent solutions, though the nature and degree of this conservatism varies with the input parameters. Further, the Rankine equations yield invalid and sometimes nonsensical solutions for ascending backfill slopes in excess of the soil friction angle, and for descending slope backfills, which may be observed by comparison to other methods under identical parameters. Yet, due to the assumptions of material incompressibility and elasticity, the solutions provided by the Rankine method are typically seen as more reliable for brittle soils rather than ductile soils, which is somewhat ironic given that Rankine's method ignores the effect of cohesion, a common strength component for brittle soils.

Bell (1915)

Bell (1915) modified the Coulomb and Rankine analytical solutions for lateral earth pressures to include the effects of cohesion, which were previously ignored. Bell postulated that cohesion impacts lateral earth pressure (for both, active and passive cases) as a function of the square root of the corresponding earth pressure coefficient. Equation 3.5, as proposed by Bell, demonstrates this relationship for passive pressure conditions. The addition of cohesion to the total passive resistance is depicted in Figure 3.2.

$$\sigma'_p = K_p * \gamma' * h + \sqrt{K_p} * c' \tag{3.5}$$

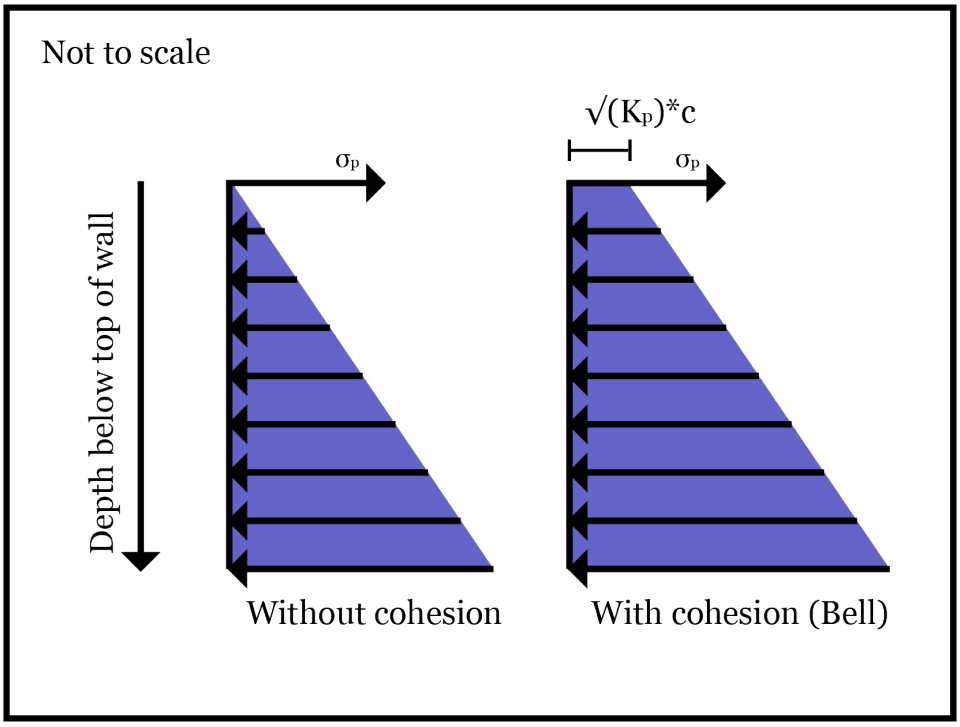

Figure 3.2: Comparison of passive earth pressure distributions with and without the inclusion of cohesion effects

Modern Empirical, Analytical, and Numerical Solutions

Terzaghi (1943)

Similar to his theory of soil bearing failure, Terzaghi (1943) proposed a curved shearing surface (i.e., failure surface) in retained soils as active or passive lateral pressures act on the retaining system. This concept is in better agreement with many observed failure planes in load tests and case studies (Chugh, 1995), as opposed to the linear planes used in the earlier Coulomb and Rankine methods. Terzaghi adopted a log-spiral shape for the failure plane, wherein a curve's path rotates about a center point with its radius increasing as a function of angular rotation. Equation 3.6 presents the generalized equation in polar coordinates (R, θ).

$$R = R_0 * \exp\left[\theta * \tan(\varphi')\right] \tag{3.6}$$

According to Terzaghi, the shape of the soil failure surface consists of a log-spiral shape until the tangent angle reaches the equivalent Rankine failure plane angle, thereafter proceeding linearly until reaching the backfill surface. This change in plane development is due to the vertical shear force applied at the wall-soil interface, which is thought to be completely dissipated in the backfill at a distance equal to half the total failure wedge length. Thus, Terzaghi's failure model may be thought of as the sum of two soil blocks--the curved zone known as the *Prandtl zone*, and the linear failure zone known as the *Rankine zone*. Figure 3.3 depicts a generalized log-spiral-based passive resistance model with its geometric relationships.

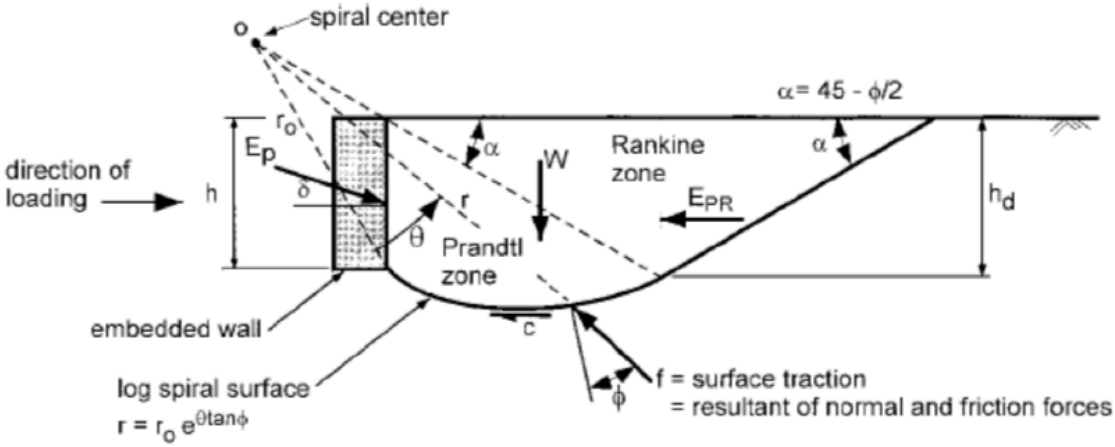

Figure 3.3: Log-spiral passive wedge model as proposed by Terzaghi (Duncan and Mokwa, 2001)

For a given initial radius, the shape and location of the corresponding failure plane may be evaluated, after which that failure wedge may be discretized into vertical slices, as shown n Figure 3.4. Given a sufficient number of slices, the shape of each slice may be

approximated as a simple polygon, making it relatively simple to evaluate the forces on each slice throughout the wedge, congruent with slice methods known in slope stability. The net forces on each slice may be then considered in summation to determine the resultant wall force for that trial. Multiple trials are attempted by varying the initial radius to converge on the critical lateral wall force (minimum for passive force, maximum for active force).

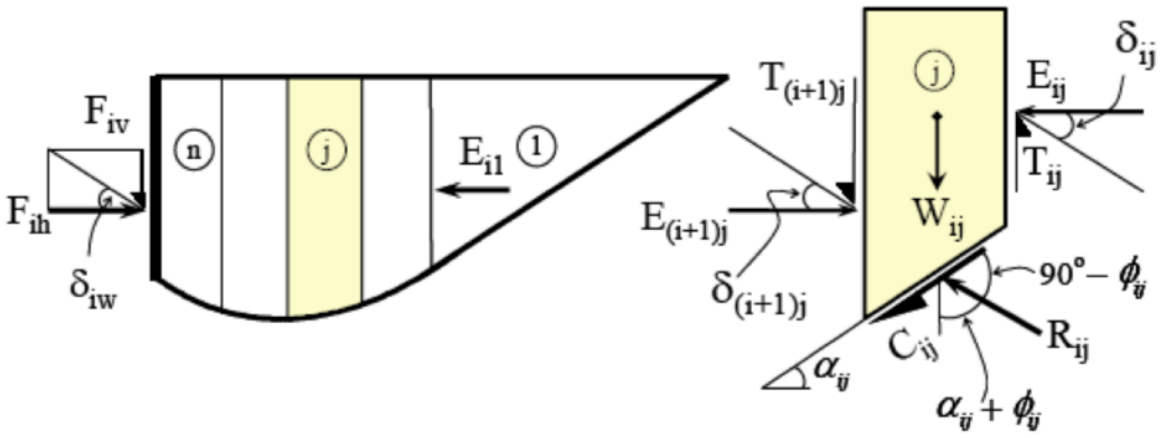

Figure 3.4: Backfill slice discretization and force equilibrium (Shamsabadi 2005)

Terzaghi and others have used multiple case studies to show the effectiveness of the *log-spiral* computation method in capturing the shape and overall response of a laterally stressed soil strata; as such, it is often considered the most accurate numerical solution to static lateral earth pressures. Nevertheless, the calculations involved in evaluating the critical log-spiral surface are both complex, tedious, and often lengthy if the solution does not converge quickly. However, later researchers such as Shields and Tolunay (1973) demonstrated how analytical geometry may be used to simplify the iterative procedure to evaluate the failure plane shape (and thus the passive earth pressure solution).

The availability of modern computer-based analysis has eased these frustrations, although optimized slice and FEM solutions have largely eclipsed the *log-spiral* method, due to the ease in accommodating unusual model configurations and/or failure plane shapes.

Optimization Solutions

The concept of optimizing a weakest plane in a backfill soil is not unique to the methods of Coulomb or Terzaghi. Similar methods were proposed by Cullman (1886) and employ multiple trial solutions which are used to develop a relationship (usually plotted graphically) between backfill geometry and ultimate passive resistance. Simpler computer-based analyses often rely on optimization of earth resistance via multiple trials using slice discretization to calculate earth pressures for section and failure plane geometries of varying complexity.

Finite Element Analysis

More complex than optimized slice analysis, Finite Element Analyses (FEA) take advantage of discretizing the backfill soil into a set of 2D or 3D elements, which each are assigned constitutive material relationships in accordance with the global model. By evaluating the stress state of each element, and summing the elements together, one may derive a more realistic understanding of the global forces at play on a body undergoing some mechanization or stress. FEA is ideal for digital computation, as the stress and strain interactions of the various individual elements are evaluated together through matrices relating to nodal forces and moments, primarily as a function of their relative stiffness and

any applied parameters or boundary conditions (such as surcharges, degrees of freedom, etc.). Evaluating these matrices as a sequential linear algebra system allows the software to evaluate the stress state (and related properties) on both the global and internal levels, a possibility not seen in the other discussed methods. Though considered the most precise and detailed means of evaluating strengths/stresses (including lateral earth pressures) in soil models (as well as many other modelled systems of other disciplines), FEA is typically considered not user-friendly and nearly always requires the time and cost-intensive use of specialized computational software.

Mobilized Development Solutions

Finite Element Analysis

Just as finite element methods may be used for detailed evaluation of the passive resistance of a retaining wall system, they can also be used to predict the wall's corresponding deflection behavior. Software like RS^2 by RocScience relies primarily on a bilateral stiffness models, where the stress-strain relationship is assumed linear until a peak stress, and flat thereafter--what is referred to as elastic perfectly-plastic behavior modelling. This stress-strain relationship is demonstrated in Figure 3.5, wherein a sample stress strain curve is compared to its bilinear approximation. While the reader may observe that the general shape and magnitude of the stress-strain curve is matched, the model fails to capture the post-peak strain softening that is common in brittle and overconsolidated, dilatent soils.

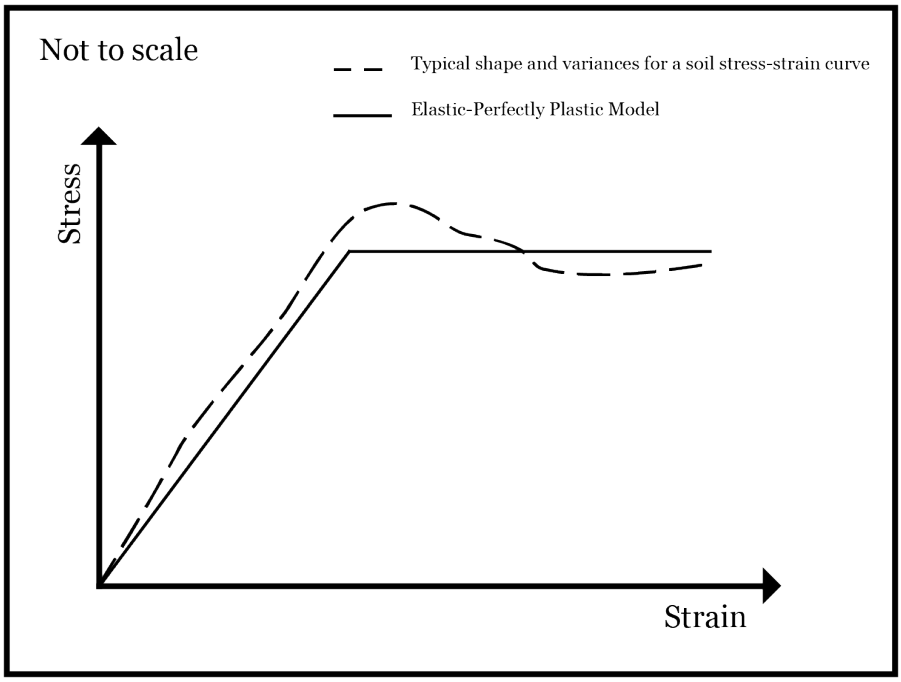

Figure 3.5: A sample experimental stress-strain curve with its bilinear model

This peak-residual stress relationship may be captured through a slightly more detailed model, wherein distinct peak and residual shear strength parameters are inputted, along with corresponding equivalent stiffnesses. Hence, once an element exceeds peak strains that element assumes the residual strengths and stiffness.

Duncan and Mokwa (2001)

Duncan and Mokwa (2001) proposed a hyperbolic load-deflection behavior relationship for the passive resistance of simple walls as described through Figure 3.6, and Equation 3.7, where P = passive resistance [force], y = deflection [length], K_{max} = initial load-deflection stiffness (force/length). R_f is called the *reduction factor*, which is the ratio between the ultimate force and the limiting asymptote of the hyperbolic curve, which is an

experimentally derived and/or assumed value usually in the range of 0.75-0.95 per Chang (1970). K_{max} is approximated based on estimated soil properties as proposed by Douglas and Davis (1964). As such, this method is less precise than FEA solutions for the evaluation of load-deflection behavior, and limits a load-deflection solution to a hyperbolic shape, without the ability to model dilatency or other curve shape irregularities.

$$P = \frac{y}{A+By} = \frac{y}{\frac{1}{K_{max}} + R_f * \frac{y}{P_{ult}}} \tag{3.7}$$

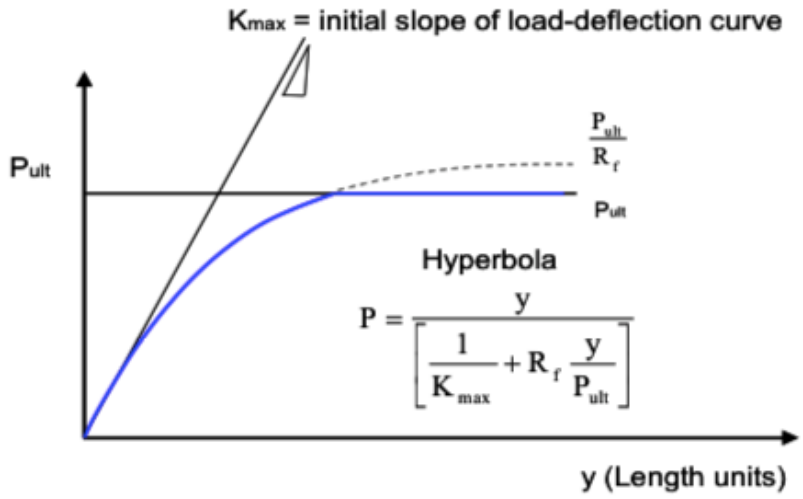

Figure 3.6: Hyperbolic load-deflection model from Duncan and Mokwa (2001).

Shamsabadi, et al. (2005, 2007)

Shamsabadi, et al. adapted the concept of stress level correlations from deep foundation lateral deflection modeling to retaining wall behavior under passive pressure conditions. Ashour, et al. (1998) originally proposed the concept of *stress levels* with respect to pile foundation lateral behavior, wherein both strength and strain values may be related proportionally to the values corresponding to the peak resistance. The stress level may be used as a common index to perform parallel strength and displacement calculations to evaluate the load-deflection behavior of a laterally-loaded structure, using a conventional log-spiral failure mechanism. As stress levels increase towards the peak resistance, the corresponding passive resistance and deflection values, when plotted together, create a hyperbolic shape, which is why the method is referred to as the *Log-Spiral Hyperbolic* model, or LSH. Normalization of values with the stress level as an index provides the analyst with a simple means of evaluating capacity; for example, wall deflection calculated at a stress level of 0.5 corresponds to deflection when the wall is loaded to 50% of its maximum capacity. Figure 3.7 shows Shamsabadi's load-deflection curve model, which uses the same hyperbolic formula as Equation 3.7, but with A and B factors as follows:

$$A = \frac{y_{max}}{2*K_{50}*y_{max}-P_{ult}} \tag{3.8}$$

$$B = \frac{2(K_{50}*y_{max}-P_{ult})}{P_{ult}(2*K_{50}*y_{max}-P_{ult})} \tag{3.9}$$

where K_{50} is the initial stiffness, obtained by connecting the load deflection relationship from its origin to 50% of ultimate capacity as shown in Figure 3.7, y_{50} is the corresponding

displacement to the point of 50% P_{ult} on the load deflection curve, P_{ult} represents the ultimate passive resistance along the curve, and y_{max} is the corresponding displacement measure at point P_{ult}.

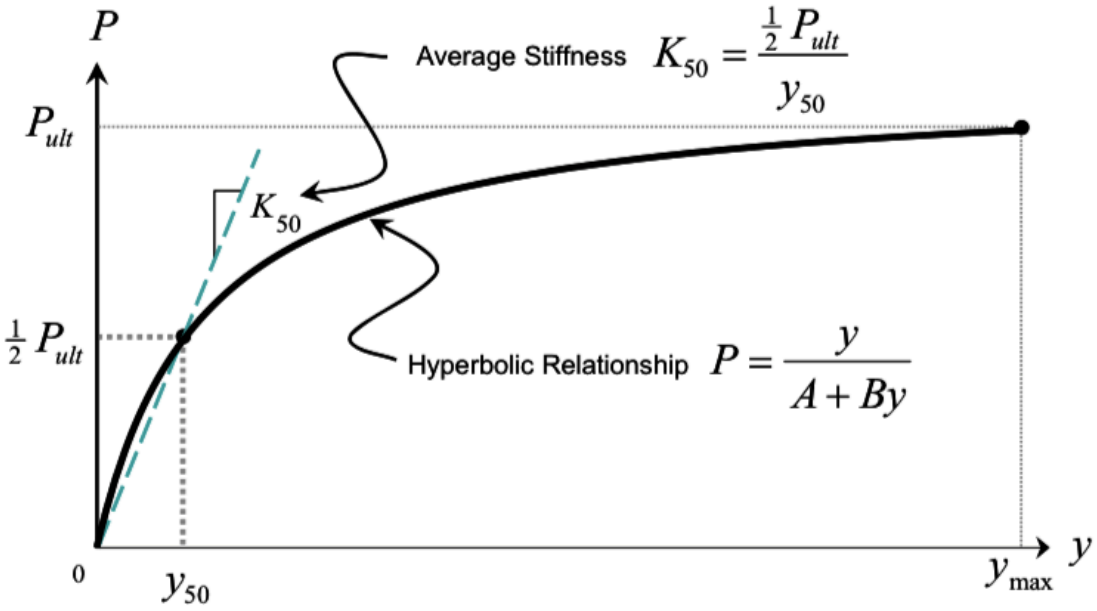

Figure 3.7: Log-Spiral Hyperbolic (LSH) load-deflection curve as proposed by Shamsabadi (2005, 2007)

Similarly to Duncan and Mokwa's method, the *LSH* method assumes a hyperbolic load-deflection relationship, which is often acceptable for design-level loading where residual strengths are not intended to be reached. The *LSH* method relies more heavily on tested soil parameters than the more correlation factor-driven methods that precede it. Nevertheless, the deflection calculation procedure assumes that deflection is solely the product of shear strains along the failure plane, and ignores any axial strains that may occur in the failure wedge or the surrounding backfill soils.

Medina, et al. (2010)

Medina (2010) proposed a simplified method for evaluating the peak displacement of a passively-loaded horizontal earth column. By discretizing the soil into vertical slices and evaluating the stress increases in each slice due to the wall loading, a displacement relationship may be derived as function of the inverse peak stiffness of the soil. This relationship is summarized in Equation 3.10, where M_{hi} is the inverse stiffness and Δx is the width of each slice. The relative compression for each slice is evaluated and then summed together, resulting in a total displacement for the given passive loading.

$$\delta y = \sum_{i=1}^{n} M_{hi} * \Delta\sigma_{hi} * \Delta x \tag{3.10}$$

Stress increases are evaluated using an influence factor method originally proposed by Zeevaert (1983) and modified by Medina (2010), where I_{FH} is the horizontal influence factor of the wall pressure on the soil:

$$\Delta\sigma_h = \sigma_p * I_{FH} \tag{3.11}$$

The resulting influence factors are multiplied by the average horizontal wall stress increase to evaluate the stress increases in each slice. While this method was proposed as a means of evaluating compression of a passive wedge at geostructural equilibrium, it may be adapted to provide a more complex analysis of load-deflection behavior in passive-resisting backfills.

4 PROPOSED METHOD

Conceptual Approach

In order to develop a solution to describe the mobilization of passive resistance with respect to lateral wall displacement, two criteria must be sufficiently understood: (1) the strain-dependent shear strength behavior in the backfill soil, and (2) the stress propagation in the backfill wedge.

In general, laboratory shear tests provide strain-dependent strength data in the form of stress-strain curves. Triaxial testing specifically provides reasonable stress-strain behavior data for a test configuration similar to the conditions along the failure plane of a retaining wall backfill. Hereby, the major compression stress corresponds to the horizontal loading onto the backfill, and the minor stress is analogous to the vertical overburden pressures. The overall failure plane is typically diagonal; however, its characteristics are dependent on the level of compaction, confining stresses, and inherent shear characteristics. Furthermore, output data from triaxial shear testing is influenced by the condition and properties of the tested sample, such as soil dilatency, grain size distribution, moisture conditions, and even expansive soil swelling pressures (though this discussion will address only granular, nonexpansive soils). Typically, however, only peak strength values are retained for shear strength computation in triaxial testing, regardless of strain behavior—thus stripping the final strength output of any strain or "performance"-based information.

Using concepts of laboratory-derived mobilized shear criteria as developed by Schmertmann (2012), the relationships between mobilized Mohr-Coulomb shear resistance axial strain can be derived from triaxial stress-strain curves. Whereas standard

triaxial testing takes the confining stress and peak compression stress for each sample as respective major and minor principal stresses and projects a tangent line to determine the shear stress failure envelope, the calculation of the mobilized shear envelope consists of fixing the sample's confining stress as the minor principal stress, and setting the major principal stress as equal to the compressive stress applied at each node along a discretized stress-strain curve. In this manner, a unique Mohr circle is created at each strain interval. This procedure is repeated for each individual triaxial test, so that at each confining stress, a suite of Mohr circles over the range of strains can be developed. Figure 4.1 below depicts a sample suite of such shear envelopes.

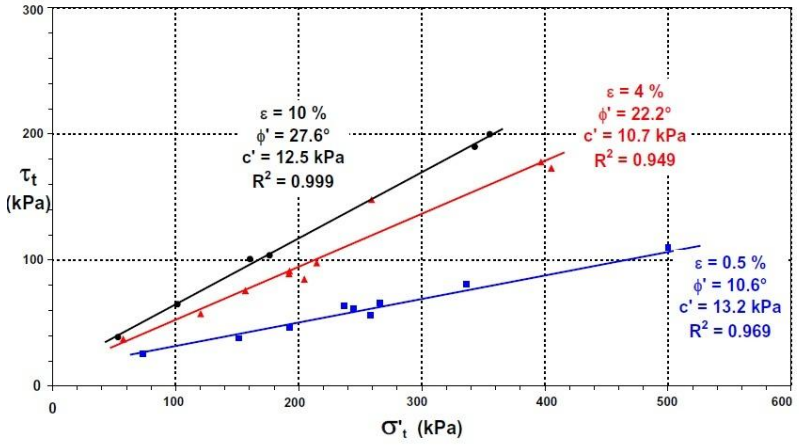

Figure 4.1: Mobilized Mohr-Coulomb shear envelopes for Boston Blue Clay at three strain levels (Schmertmann 2012)

Typically, three triaxial tests on three soil samples are conducted. The stress states for each sample at 0.5% axial strain would be used to develop a Mohr-Coulomb shear envelope (and thus derive ϕ and c) corresponding to that specific strain level. This process is repeated at 1.0% strain, and again until residual-level strain is reached. The resulting

shear strength envelope may be visualized as shown in Figure 4.2, as a three-dimensional function with respect to axial strain and normal stress.

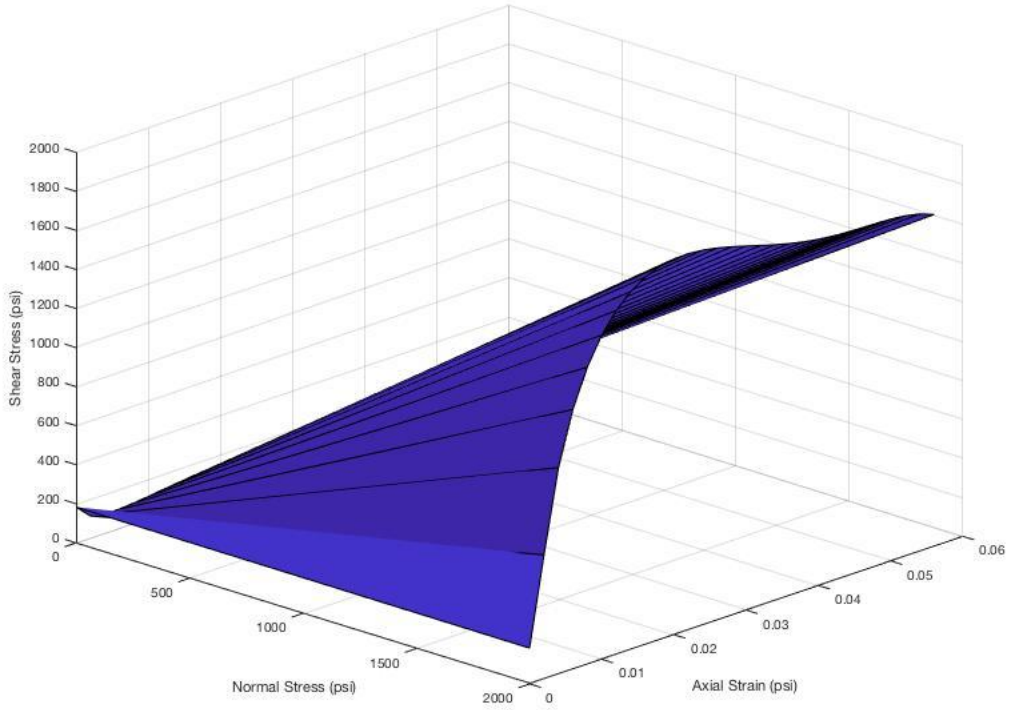

Figure 4.2: Three-dimensional representation of mobilized shear strength envelope with respect to axial strain and normal stress

With representative mobilized shear strength now defined from the above analysis procedure, attention must be turned to modeling the stress development and transmission throughout the wedge body. While a basic triangular Rankine- or Coulomb-type passive failure wedge may be simplified to a small collection of vector forces and solved deterministically, failure wedges are rarely ever perfectly triangular but are more often curved as suggested by Terzaghi (1948). As such, a log-spiral approach is proposed for various mobilized shear strength data sets corresponding to unique axial strain values

ranging from zero to the point of ultimate failure. Once passive pressures with respect to axial strains are developed, the method proposed by Medina may be used to evaluate the horizontal wall displacement for each evaluated strain increment. This procedure proposed is unique in that, unlike the hyperbolic model methods (Duncan and Mokwa, 2001 and Shamsabadi et al., 2005), a load-deflection shape is not prescribed to the wall, while mobilized soil strengths and stiffnesses adapts the simplicity of the Medina et al. comp

Proposed Procedure

Mobilized Passive Earth Pressure Calculations

1. Triaxial Shear Testing

Shear testing should be conducted using triaxial shear testing methods as outlined in ASTM D 4767 for *Consolidated Undrained* samples (*CU*), or for *Consolidated Drained* samples (*CD*). In the *Consolidated Drained* method, a cylindrical sample of representative soil is allowed to consolidate from the applied confining stress, and is then axially stressed whilst the sample (sealed inside the membrane) remains open to equilibrium with atmospheric pressure. This mitigates any global accumulation of pore pressures within the sample; meanwhile, the sample is sheared at a very slow rate (less than 0.2% axial strain per minute) to minimize localized pockets of pore pressure buildup. The *Consolidated Drained* method is similar in process, though the sample may not be sheared at a slow rate, and the sample is pneumatically sealed, allowing pore pressure to develop within the enclosed sample. Nevertheless, pressures within the sample may be measured and recorded, and subtracted from the measured stresses, with the resultant reflecting the strength contributions from the soil itself.

Regardless of the method employed, the intent is to capture the isolated shear strength of the soil sample itself, which, in the case of bridge abutments and many retaining structures, is granular material and thus subject primarily to *drained* loading conditions. Additionally, a minimum of three (3) tests should be run (in convention with common engineering practice) at unique confining stresses representative of in-situ loading conditions encountered within a backfill section (before being subjected to loading). Doing so minimizes errors associated with fitting linear or otherwise simplified failure envelopes to nonlinear or complex shear strength data by limiting the data set to the range of interest.

Triaxial shear testing requires remolding laboratory samples to unit weights and moisture contents representative to those encountered during the execution of the lateral load tests (e.g., for research studies). This, however, is often not the case for laboratory shear testing conducted in engineering practice (i.e., during mundane geotechnical design procedure), where samples are often prepared to mimic minimum acceptable standards, or critical conditions in the field; for example, 90.0% relative compaction under full saturation. Thus, it is reasonable to assume that an analysis would employ sample conditions that would result in conservatism in measured shear strength, which would then propagate throughout the analysis. More realistic results however, would be obtained with shear tests that more closely mimic in situ conditions.

Upon completion of the shear testing, appropriate corrections are made for pertinent testing conditions, such as sample dimension proportions, influence from the membrane enclosing the sample during testing, areal corrections from radial strain development, as in accordance with ASTM standards. If samples are tested under *CU* conditions, pore pressures should be subtracted from the measured axial and radial

stresses (σ_1 and σ_3, respectively). The resulting data should be presented as a relationship between *axial strain* (ε_a), *effective confining* (minor) *stress* (σ'_3), and *principal stress difference* (σ'_1-σ'_3), also referred to as the *deviator stress*.

2. Mobilized Shear Strength Envelope Analysis

In general accordance with the method suggested by Schmertmann (2012), triaxial data is processed to develop unique shear failure envelopes for various strain levels, thus providing a relationship between strain development and shear strength development for the sampled soil (as in Figure 4.2). For the purposes of the analysis presented herein, the Mohr-Coulomb linear failure criterion was chosen due to its ease of use and prevalence in geotechnical analysis. For each desired strain level, the corresponding average mean stress is calculated according to the following equation:

$$\underline{\sigma'} = \frac{2\sigma'_3+\sigma'_1}{3} = \frac{3\sigma_3+PSD}{3} \tag{4.1}$$

For each strain interval, a linear regression is run on the three (or more, if more samples were tested) sample data points, taking the average mean stress as the independent variable. The relationship between average mean stress and principal stress difference is commonly referred to as a *P-Q relationship*, and may be plotted on a two-dimensional graph for visual review and comparison, as shown in Figure 4.3. Readers familiar with liquefaction triggering theory may note that *P-Q* diagrams are often used to analyze stress paths and strain hardening relationship in potentially liquefiable soils.

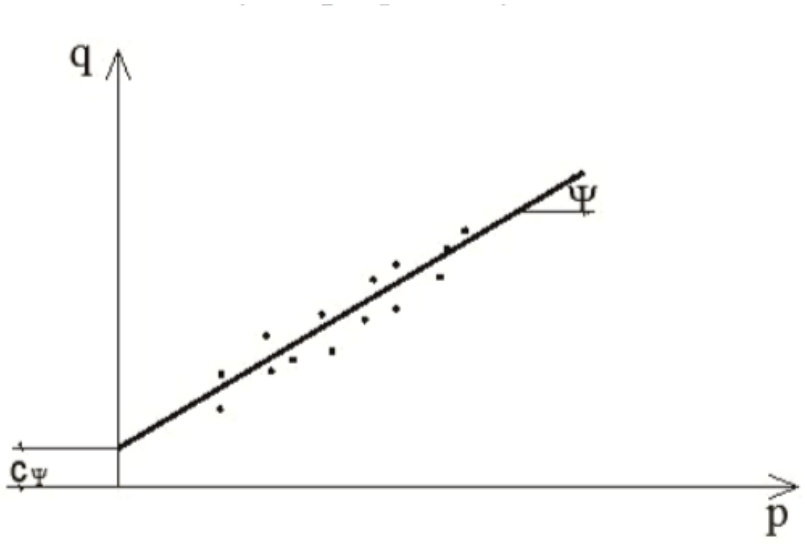

Figure 4.3: P-Q graph of triaxial test data (Amšiejus, 2010)

The linear fit equation for the *P-Q* stress path must be represented in *slope intercept* form as follows:

$$Q = m * P + b \text{ or } PSD = m * \underline{\sigma'} + b \tag{4.2}$$

With the stress path represented by this linear relationship, the slope, *m*, and intercept, *b*, may be translated into Mohr-Coulomb failure criterion parameters φ' (*effective friction angle,* units in degrees) and *c'* (*effective cohesion*, units in force per area), according to Equations 4.3 and 4.4:

$$\phi' = sin^{-1}(\frac{3m}{6+m}) \tag{4.3}$$

$$c' = \frac{b*tan(\phi')}{m} \tag{4.4}$$

The corresponding Mohr-Coulomb failure state equation,

$$\tau' = \sigma' * tan(\phi') + c' \quad (4.5)$$

may be plotted against Mohr stress circles of each test sample to compare for a reasonable data fit.

After repeating this procedure for each desired strain increment, the relationships between (1) ε_a and φ', and (2) ε_a and c', may be compared. Assuming triaxial test results are relatively consistent, plots of ε_a versus φ' and ε_a versus c' should follow a development trend similar to the stress strain curve shapes from each triaxial sample. The corresponding Mohr-Coulomb parameter development relationships with respect to strain may be used in their discretized state for the purposes of analysis, though if the strain increments used for the actual backfill analysis vary from those used in the development of the mobilized shear profile, then polynomial function fitting may be utilized to represent the development of φ' and c' with respect to ε_a.

3. Wall Section Geometry

Figure 4.4 shows a typical wall and backfill section configuration. For a simplified analysis, the wall is represented as a rectangular gravity wall without a footing, to avoid any effect of a footing on the passive pressure development. The wall is pushed into the backfill at one-third of the wall height, measured from the ground, to mirror the resultant force of a triangular reaction pressure distribution from the backfill. As inertial effects are to be ignored, the mass of the wall is assumed to be zero, and is included in the graphical depiction for illustrative purposes only.

A common coordinate system must be established to discretize the wall backfill into slices and facilitate comparison between passive pressure calculations for different strain increments. This paper assumes the origin to be located at the heel of the wall, so that most, if not all, of the backfill section in the first quadrant where failure occurs.

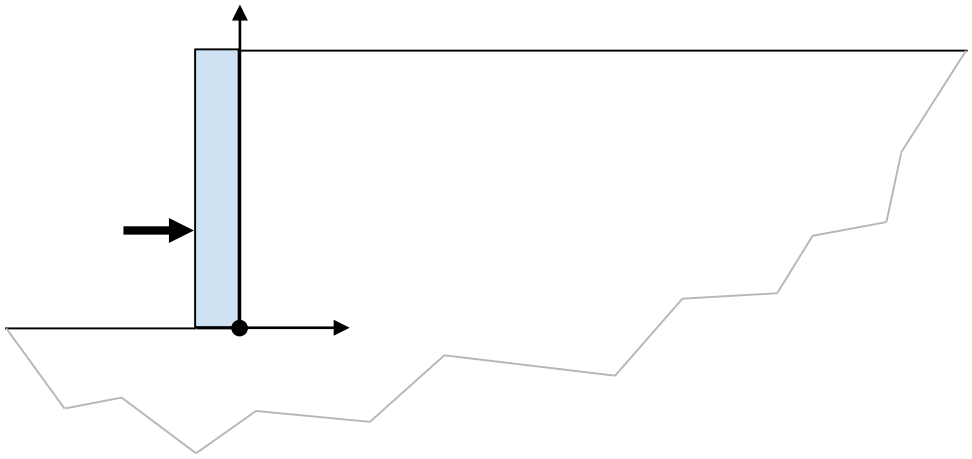

Figure 4.4: Generic retaining wall section with coordinate system assigned

4. Failure Plane Evaluation

While various force- or moment-equilibrium methods for evaluating passive earth resistance of a soil wedge may be applied (Coulomb, for example), Terzaghi's method (1943) evaluates the passive resistance of a curved ("log-spiral") failure surface, which has been shown to correlate well with load tests in terms of total resistance and geometry, as documented through in many load test experiments since Terzaghi (1946).

Figure 4.5 depicts the geometry of a log-spiral passive failure plane in a retaining wall backfill. The failure begins at the base of the wall and develops radially around point *O*, with the radius of the arc increasing according to Equation 4.6:

$$r = r_0 * e^{tan(\phi)} \tag{4.6}$$

When the radius of the failure plane reaches angle α, which is equal to

$$\alpha_1 = 45° - \frac{\phi'}{2} \tag{4.7}$$

The failure plane proceeds as a linear plane until it reaches the surface of the backfill. Terzaghi hypothesized that nonlinearities in failure wedge geometry are the result of interslice shear created by friction between the wall and the backfill. This interslice force dissipates linearly, reaching zero when the log-spiral shape tangents the Rankine failure plane angle (Rankine's earth pressure analysis is based on plasticity theory for backfills with frictionless wall interfaces). Given this shape, point *O* is moved along a projection of line *AD*, with the failure wedge shape and passive resistance calculated iteratively until the passive resistance is optimized to a minimum, corresponding to the shape and strength of the critical failure plane. The Shield and Tolunay (1973) method may be used to simplify calculations by avoiding repeated optimization cycles.

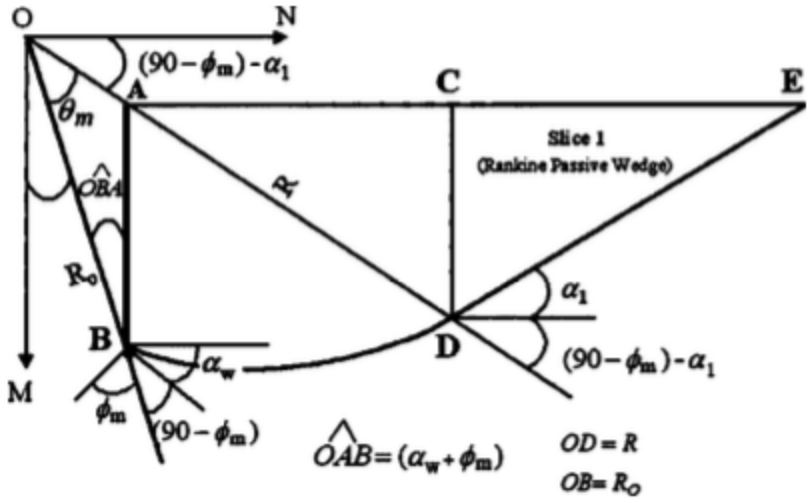

Figure 4.5: Log-spiral passive wedge geometry (Shamsabadi et al., 2005)

5. Slice Discretization

After developing the shape of the failure plane, the wedge formed by the plane must be discretized into slices in order to analyze the force propagation of the system. While others have proposed optimal discretization for the analysis of force equilibrium in earth structures, a total of five slices are proposed for this method—four in the log-spiral zone, and one for the Rankine wedge. The assumption of five slices is based on experimentation, as increasing the number of slices beyond five did not appreciably impact the resultant force. Given that, in the log-spiral earth pressure theory, vertical friction is null in the Rankine wedge portion, it is superfluous to analyze this portion of the passive body with any finer resolution than a single sliding block, as under standard assumptions normal and shear forces develop linearly along a linear failure plane.

6. Passive Earth Pressure Calculation

The passive earth pressure is evaluated by analyzing axial and shear forces in both planar dimensions, and moment in the projected dimension (under plane-strain criteria) for each respective slice. The sum total of the slices represents the total strength of the backfill. Assuming the nomenclatures of Figure 4.6, the force and moment equilibrium yield a passive force contribution for each individual slice in agreement with Equation 4.8, per Shamsabadi.

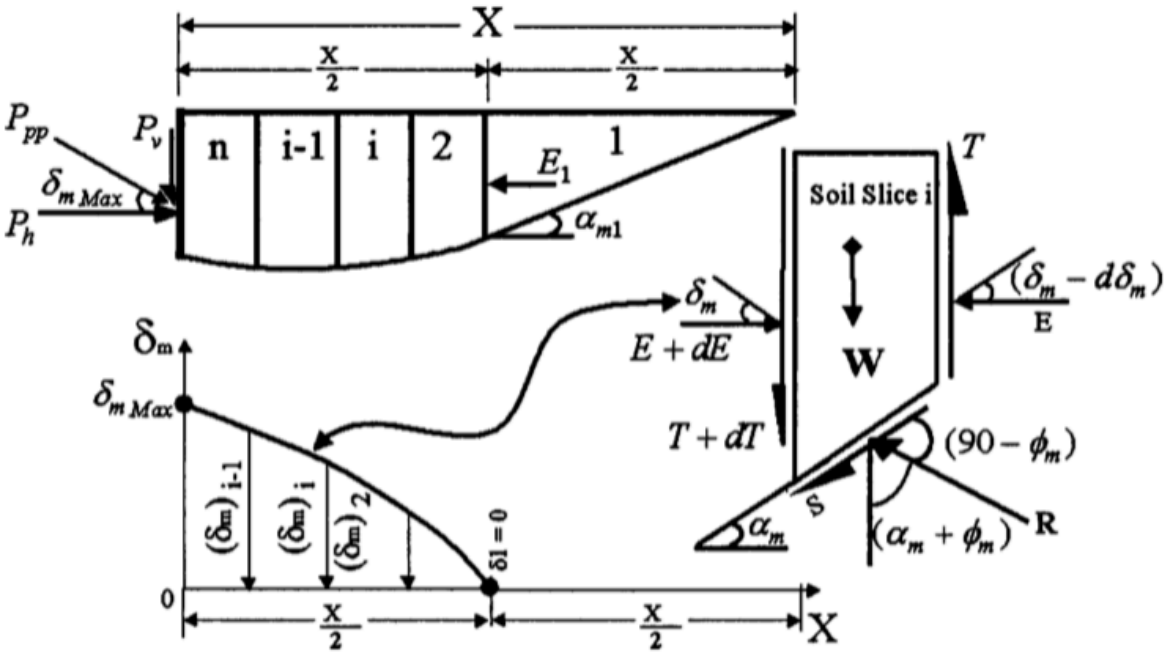

Figure 4.6: Log-spiral force block diagrams (Shamsabadi et al., 2005)

$$dE = \frac{W*\tan(\alpha_m+\varphi_m)+c_m*L*(\sin\alpha_m*\tan(\alpha_m+\varphi_m)+\cos\alpha_m)}{(1-tan\delta_m*\tan(\alpha_m+\varphi_m))} \qquad (4.8)$$

Given that, for a quadrilateral wedge this equation is indeterminate (unknown forces are applied on both the left and the right vertical faces), the analyst must begin with the Rankine failure wedge, and work through each successive slice until reaching the wall.

Since the Rankine wedge is triangular, there is only one vertical face for forces to act on, allowing the above equations to be evaluated deterministically when performed in sequence, as the forces on the left face of one slice are equal and opposite to the forces acting on the right face of the adjacent slice, and so on. The resulting force represents the total passive earth resistance in units of force per length of wall, which may be translated into total force (when multiplied by the length of wall), or deconstructed into earth pressure coefficients, equivalent fluid pressures, etc.

7. Iteration

Once steps 4 through 6 have been performed for the initial strain increment, they should be repeated for each successive strain interval until a relationship between passive earth resistance and triaxial test strain has been developed across the desired range. Upon completion, the analyst will be able to compare failure plane and passive earth resistance development as the backfill soil mobilizes.

Displacement Calculations

Axial stress-strain curves from the triaxial testing may be referenced to evaluate the displacement characteristics of the backfill soil at each analyzed increment. Similarly to the evaluation of earth pressures, the compression data should model the assumed field conditions of the backfill. Consiolidated-Drained testing or pore pressure correction should be used on walls which are assumed to be loaded slowly, while undrained conditions may be modeled by CU triaxial curves that are not corrected for pore pressure.

It is crucial to understand that for the evaluation of passive strength, the slice discretizations are based on the evaluated *weakest* plane, so the triaxial strain values associated with each iteration of passive earth pressure evaluation are indicative only of the normal strains on and immediately surrounding the failure plane. These strain values are thus only meaningful as an index for the corresponding passive resistance values; without evaluation via computer analysis, a separate analysis must be performed to evaluate displacements. The following steps outline the proposed method for evaluating the wall displacements associated with mobilized passive response of an abutment wall.

1. Backfill Discretization

Following the method proposed by Medina (2010), an assumed horizontal soil column of backfill is discretized into vertical slices. This system of slices different than that used for strength evaluation. The backfill area considered should encompass the entire thickness of soil behind the wall that may experience a stress increase and compress, which intuitively extends far beyond the failure wedge. As aforementioned, these slice discretizations are unique from those used for the evaluation of passive strength, as they will be used to analyze an *average* horizontal stress increases in the backfill area. To correlate the stress increases and resulting compression with the approximately exponential decreasing stress changes in soil due to loading (from the works of Boussinesq and others), the analyst may reduce the total number of slices while retaining accuracy by increasing slice width the further the distance away from the wall. This slice model should extend until stress increases are minimal (see step 2 below), at least until loading stresses decrease below 5% of the loading at the wall.

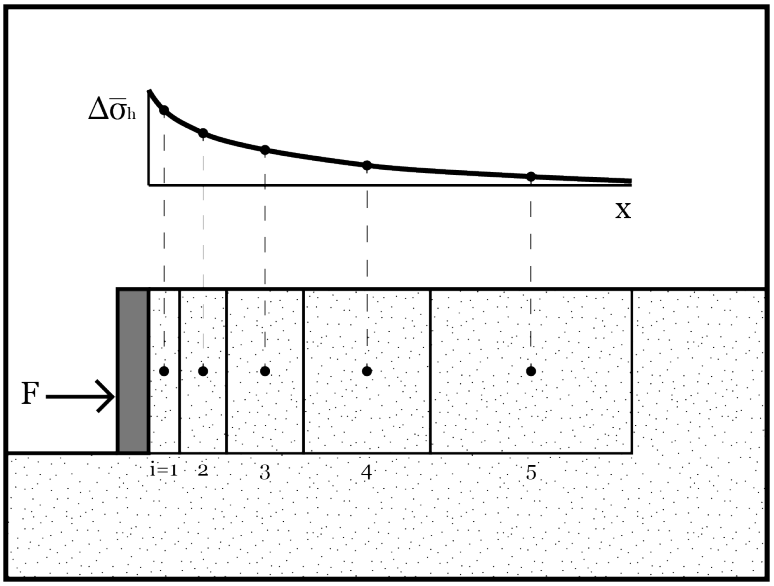

Figure 4.7: Stress increase propagation in wall backfill

2. Stress Increase Calculation

Stress increases throughout the backfill are calculated using the procedure outlined by Medina (2010), wherein influence factors are calculated for each backfill slice and multiplied by the average applied wall pressure to yield the net change in horizontal stress, similar to methods proposed by Boussinesq and others. For each slice, the geometry and applied pressure at the wall are used to evaluate the increase in horizontal stress.

3. Evaluation of Backfill Stiffness

Triaxial stress-strain curves are used to evaluate the compressive stiffness at each considered axial strain level. Since the cell pressure affects the soil response stiffness in a triaxial test, and is analogous to the resting pressures in the soil prior to loading, choose the curve from a test with a cell pressure that represents the mean vertical stress conditions in the backfill failure wedge. Stress-strain curves for the equivalent vertical effective stress at the mid-depth of the wall have been used with success in the analysis herein. If no triaxial

sample was sheared at that pressure, appropriate scaling measures may be taken, based on patterns observed in the various triaxial sample stress strain curves. Hereafter the inverse of the equivalent stiffness is determined, so it is in units of length^2/force. This results in a pseudo-elastic representation of soil strain development with respect to stress, at the peak stress value.

4. Evaluation of Displacement

The relative compression displacement of each slice is evaluated by multiplying the inverse stiffness by the stress increase and slice thickness, as per Equation 3.10. The relative displacements from each slice are then summed to derive the total displacement at the wall, presenting displacement as a function of the average horizontal axial strain in each slice, similar to evaluation of one-dimensional vertical settlement in soil strata due to foundation loading.

5. Presentation of Results

Passive resistance results may be plotted against horizontal wall displacements, yielding a load-displacement curve that may be used for design and analysis. Figure 4.8 below depicts a summary of the modelling process in flowchart form.

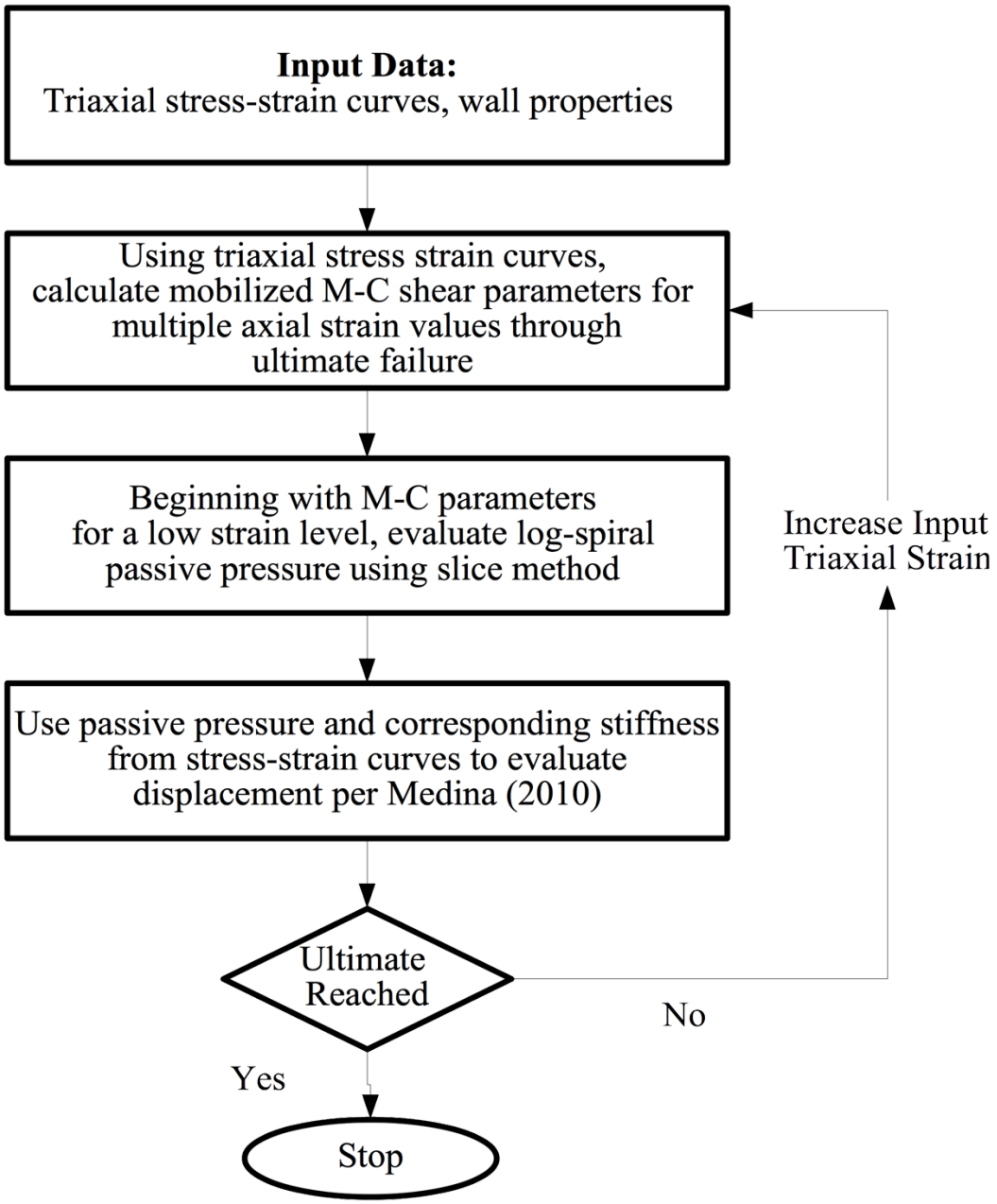

Figure 4.8: Procedure flowchart for proposed method

5 CASE STUDIES

Lemnitzer, et. al. (2009)

Lemnitzer et al., (2009) constructed a 1.68-m tall, 4.57-m long abutment wall for load testing, to compare various analytical and empirical passive earth pressure solutions with actual observed values. To correspond with Caltrans construction methods, SE30 backfill sand—granular material—was placed and compacted behind the abutment wall.

With boundary conditions set to model plane-strain conditions, the SE30 backfill sand was compacted behind the abutment wall in excess of 94% relative compaction to simulate typical field scenarios. Following construction, the completed abutment was then pushed failure, with load actuators restraining vertical wall movement. Loading was applied by a horizontal actuator in cycles, to analyze reloading stiffness. After subtracting out the contribution of base friction from the measure passive resistance (i.e., subtraction of friction due to self-weight of the abutment wall), the resulting backbone curve of passive backfill resistance reflects an ultimate force of 2210 kN at a displacement of approximately 5 cm, with a residual resistance of 2130 kN at a displacement of 11 cm. This load-displacement relationship is depicted in Figure 5.1 below.

Lemnitzer, et. al. (2012)

Following similar criteria to the earlier testing on dense backfill, Lemnitzer (2012) performed load testing on another abutment model, this time with a backfill height of 2.4-m tall by 4.57-m long. Similar, granular backfill material was used, also conforming to the SE30 specification, with an in-place relative compaction tested between 94-96%. Load test results yielded results significantly higher than predicted by the various methods

compared in the study, with an ultimate capacity of 7340 kN at a displacement of approximately 13.5 cm. As shown in Figure 5.1, the model showed residual behavior characteristics, but did not reach a steady value within the displacement constraints of the test.

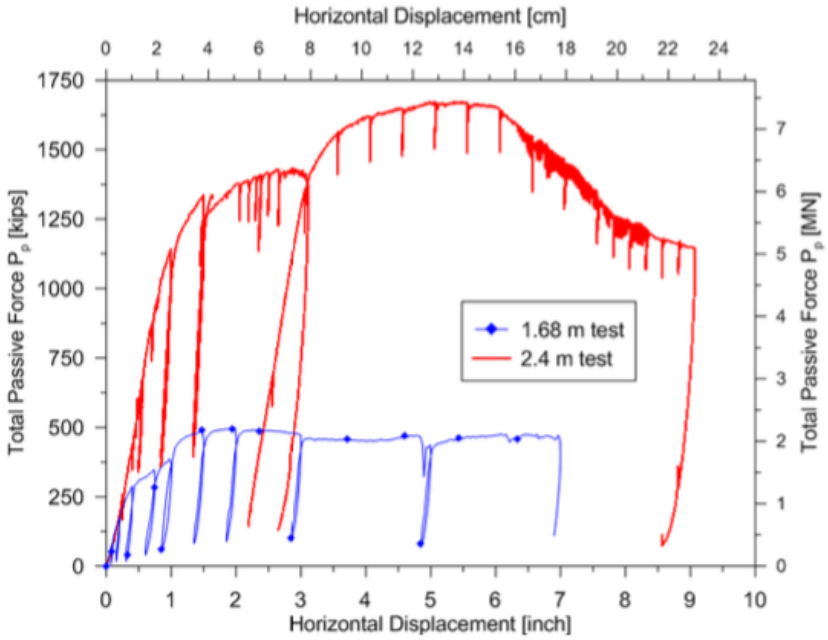

Figure 5.1: Load-deflection curves for the 1.68 and 2.44 meter tests by Lemnitzer et. al, (2009, 2012)

Wilson, et al. (2010)

Wilson et al. conducted a study using a 4.72-m long gravity abutment wall model on which two independent load tests were executed. The 1.68m high backfill consisted of a silty sand complying with CalTrans SE30 specifications, which was compacted to an average of approximately 95-96% relative compaction. Load Test 1 was conducted 20 days after completion of backfill and compaction, while Test 2 was conducted after only 3 days, thus more closely mirroring conditions used for the corresponding laboratory testing. Load testing yielded an ultimate resistance of 1,105 kN at 4.6 cm for Test 1, and 936 kN at 5.1 cm for Test 2. The stiffer, more brittle failure of Test 1 is consistent with the assumed

mechanics of cementation and drying associated with the 20-day time lapse. Both tests reached a residual resistance of approximately 608 kN at a displacement of approximately 13.5 cm. A comparison of the backbone curves for each test is shown in Figure 5.2.

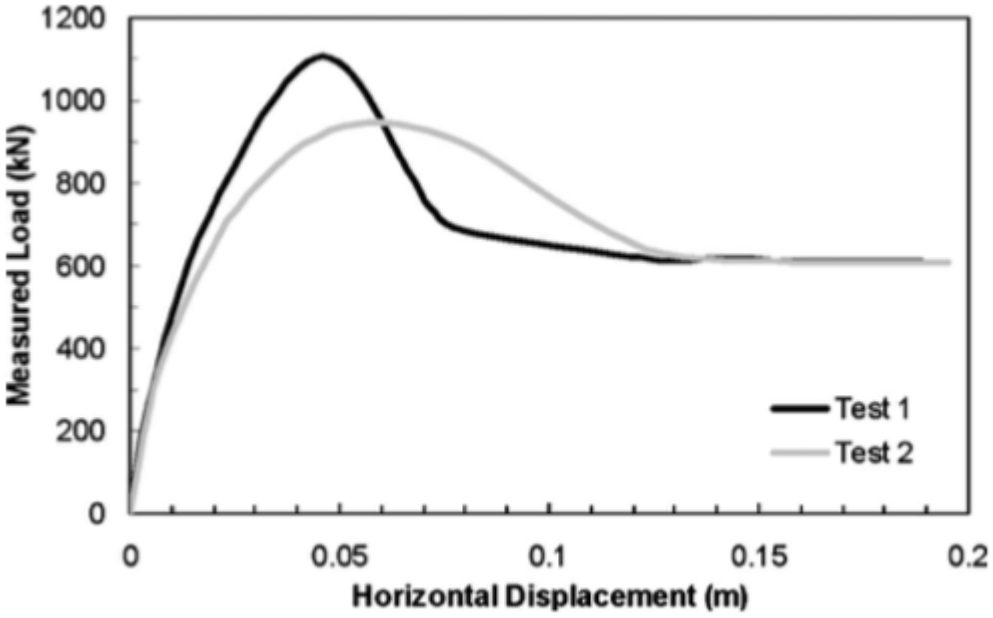

Figure 5.2: Measured load-deflection curves for two load tests (Wilson, 2010)

6 ANALYSIS

In accordance with the proposed method, the passive resistance behavior of the soil backfill was modeled for each of the three load tests previously discussed: Lemnitzer et al. (2009), Lemnitzer et al. (2012), and Wilson et al. (2010). These results are presented for comparison below. Triaxial shear testing was performed on unsaturated soils, with moisture contents and compaction selected by the original researcher to imitate field conditions of the load test.

Lemnitzer, et al. (2009)

Triaxial testing (Consolidated Undrained, subtracting pore pressures) was performed on a representative sample of backfill material. Test results yielded peak Mohr-Coulomb shear parameters of ϕ'=40° and c'=14 kPa. Deviator stress-strain curves, shown in Figure 6.1 for this shear test were evaluated to determine the *mobilized* envelope as previously described, resulting in "peak" condition M-C parameters of ϕ'_m=39.2° and c'_m=19.9 kPa at a specimen axial strain of 1.65%.

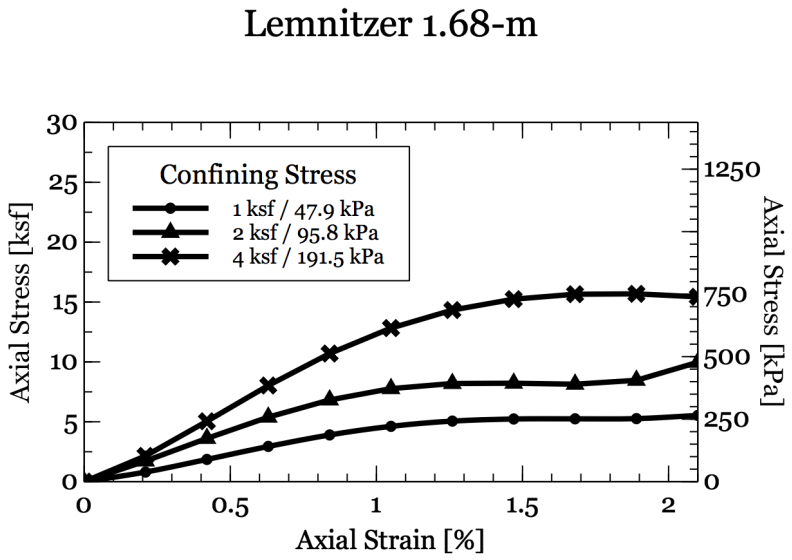

Figure 6.1: Triaxial CD stress-strain curves for backfill sample from Lemnitzer 1.68-m wall test

One problem with the triaxial data as-tested was that a "staged" test was performed, meaning that once the strength of the soil sample yielded at a given confining pressure, loading stopped, the confining pressure was increased to the next test increment, and the same sample reloaded. While this method provides accurate measurement of shear strength up to peak resistance, it does not provide any residual strength information. As such, the analysis in this particular case only applies to the development of ultimate resistance, and does not provide any meaningful estimate of residual resistance. Shear parameter development for this case is shown in Figure 6.2.

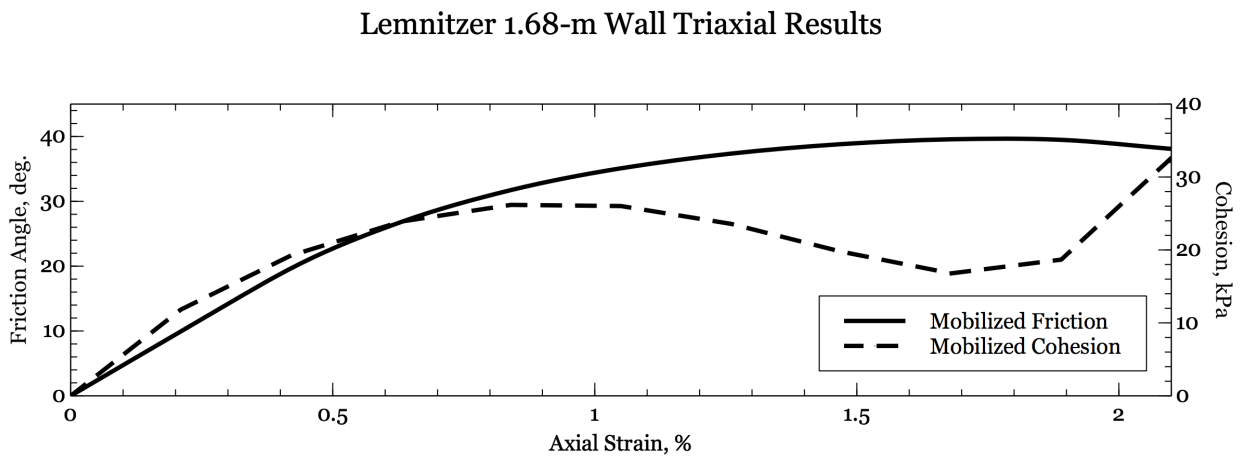

Figure 6.2: Mobilized friction angle and cohesion curves with respect to strain for stress-strain curves shown in Figure 6.1.

Following the development of these parametric relationships, the passive resistance was evaluated at four intervals representative of the shear strength development relationship; namely at axial strain levels of 0.33%, 0.66%, 0.0825%, and 1.65%. To represent the overall decrease of wall interface friction observed both, in this case study and in general, wall friction was assumed to initially be equal to the *mobilized* friction angle of 16.4 degrees at the initial calculated strain level of 0.33%, and decreasing to 15 degrees (the approximate average wall friction measured in the load test) by the 0.83% strain level evaluation.

Following the Medina (2010 procedure, the triaxial test axial strains were transposed into actual horizontal deformation of the abutment backfills. Using the deviator stress-strain data, representative stiffnesses for each calculation stage were derived by scaling stress-strain data in proportion to an average assumed confining stress in the backfill, which is assumed to be at the depth of the resultant passive force (⅓ up the backfill height). After checking the rate of stress decay, it was found that a horizontal thickness equal to four (4) times the wall length should be considered for deformation

calculations, as the stress increase due to loading at such a distance was found to be on the magnitude of up to only 1.5%. Adhering to common practice in analytical soil analysis, this backfill thickness was discretized into 10 vertical slices (compressing horizontally). Given that the boundary conditions of the test intended to model *plane*-strain conditions, a wall length of 30.5 m (100 feet) was used in the equations to approximate an infinitely long abutment. Poisson's Ratio was assumed to be 0.2, due to the highly granular nature of the backfill, though the calculation procedure appears to exhibit a low sensitivity to variations in Poisson's Ratio. The calculated slice deformations are summed as the total horizontal wall displacement. The results of each shear mobilization stage are presented in Table 6.2.

Table 6.1: Load-displacement result values for each given strain stage, Lemnitzer 1.68-m wall

Stage	*Average strain*	*Φ'_m (deg)*	*C'_m (kPa)*	*∂' (deg)*	*P_p (kN/m)*	*M (m^2/kN)*	*Δ (cm)*
(0)	(0)	(0)	(0)	(0)	0	(0)	(0)
1	0.33%	16.4	18.2	16.4	217	8.25E-5	1.93
2	0.66%	27.8	26.0	15.2	347	8.23E-5	3.09
3	0.83%	31.5	27.9	14	423	8.49E-5	3.89
4	1.65%	39.2	19.9	14	423	1.26E-5	5.76

The resulting passive resistance vs. deformation plot is compared to the load test backbone curve in Figure 6.3. As aforementioned, the analytical solution only provides a relationship up to the ultimate value in this case, due to the nature of the triaxial data used in this analysis. The discrepancy in initial stiffness may be attributed to triaxial test paramters, as discussed in more detail in Chapter 7.

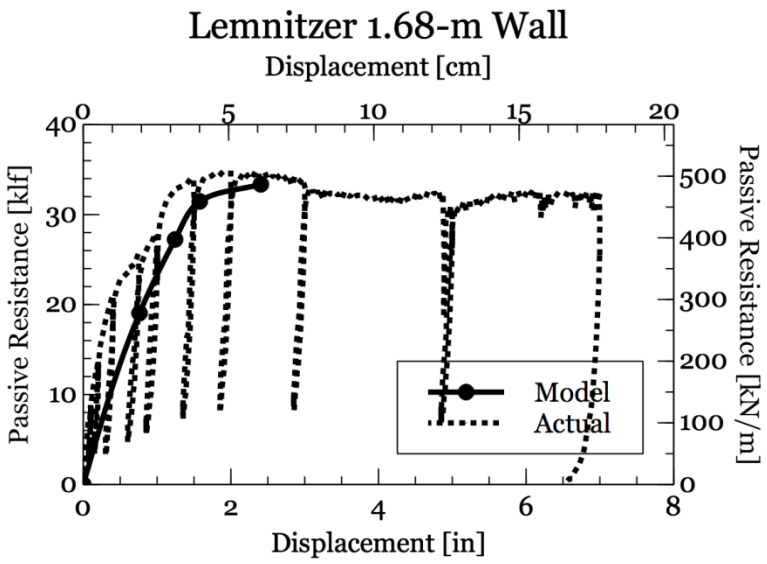

Figure 6.3: Modeled vs. actual load-deflection curves for Lemnitzer 1.68-m wall test

Lemnitzer, et al. (2012)

Using the same procedure as above, passive response of the backfill was predicted for the 2.4-m backfill test reported in Lemnitzer et al.'s 2012 paper. Triaxial stress strain curves are presented as Figure 6.4, illustrating a hyperbolic-type stress development, consistent with contractive and/or ductile soils.

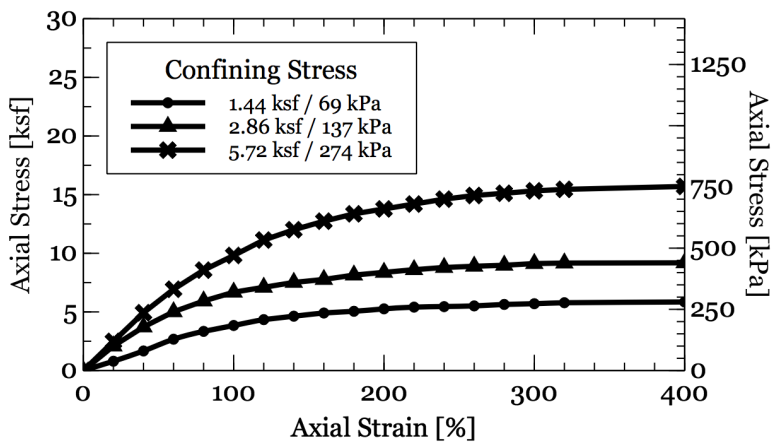

Figure 6.4: Triaxial stress-strain curves for the Lemnitzer 2.44-m wall test

Static shear strength parameters derived through consolidated drained triaxial testing were reported as ϕ'=39° and c'=24 kPa. Deviator stress-strain relationships were used to derive the mobilized shear parameter relationships as shown on Figure 6.5. These figures indicate a peak mobilized friction angle of 37.4 degrees at an axial strain of approximately 6%, with mobilized cohesion developing to a peak of 32.6 kPa much quicker, at 0.94% axial strain.

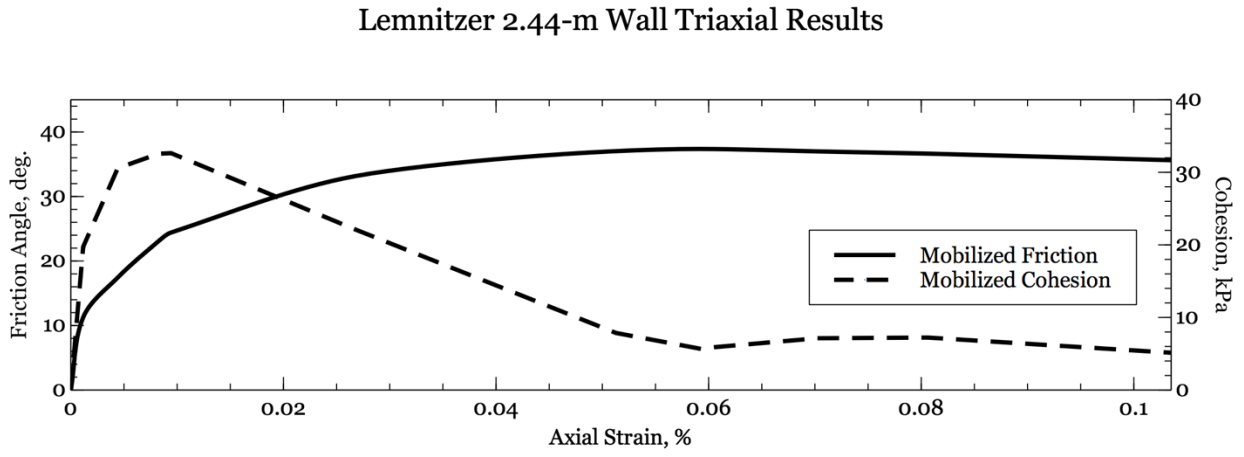

Figure 6.5: Mobilized friction angle and cohesion curves for Lemnitzer 2.44-m wall test

Table 6.2: Load displacement model data for each given strain stage, Lemnitzer 2.44-m wall

Stage	ε_a	Φ'_m (deg)	C'_m *(kPa)*	∂' *(deg)*	P_p *(kN/m)*	M *(m²/kN)*	Δ *(cm)*
(0)	(0)	(0)	(0)	(0)	(0)	(0)	(0)
1	0.116%	11.3	19.7	11.3	309	1.17E-4	1.94
2	0.441%	17.4	30.6	17.0	655	1.98E-4	7.98
3	0.826%	23.1	32.6	18.0	654	2.74E-4	12.5
4	2.68%	33.2	22.1	18.0	767	3.57E-4	43.7

Load-displacement modeling results are provided as Table 6.2. Wall friction was taken at 11.3 degrees initially to match the mobilized friction angle, increasing up to 18 degrees to correspond with the average as-measured wall friction,. Compression moduli *M* used were interpolated from stress strain curves for an overburden pressure equal to two-thirds the depth of fill behind the wall. The passive force was evaluated using five slices (four in the Prandtl zone, and one to account for the Rankine wedge), while the backfill compression was evaluated using 10 slices, each 2.44 feet wide in order to analyze a total backfill width equal to 10 times the wall height. A wall length of 30.48 meters was used for the compression analysis, to account for the plane-strain conditions the load test intended to model. The results indicate an approximate hyperbolic shape increasing up to a maximum passive resistance of 655 kN/m at a displacement of 43.7 cm, though, similar to the load test, approximately 85% of the ultimate capacity was realized within the first 8 cm. A comparison of force development and overall curve shape shows the modeled load-deflection curve to be a reasonable approximation of the actual load test. Figure 6.6 shows the resulting passive resistance calculated with respect to displacement as compared to the peak backbone of the load test results.

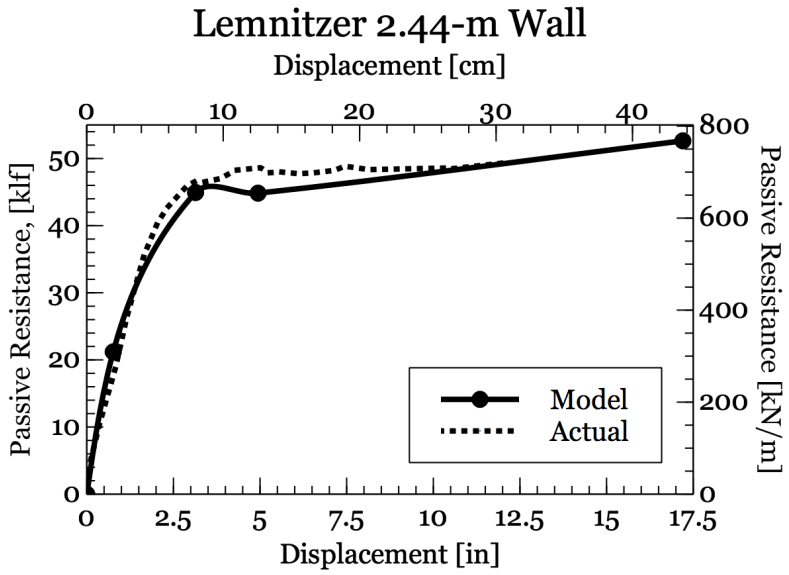

Figure 6.6: Modeled vs. actual load deflection curves for Lemnitzer 2.44-m wall test 8-01

Wilson, et al. (2010)

Consolidated drained triaxial data from Wilson's test suggests peak Mohr-Coulomb shear parameters of ϕ'=39° and c'=24 kPa. Deviator stress data was processed to provide mobilized shear information. Figure 6.8 shows the development of the mobilized shear parameters with respect to axial strain. Mobilized friction and cohesion both develop quickly to values of approximately 45 degrees and 13 kPa at 2% axial strain, with friction mostly plateauing thereafter, and cohesion steadily decreasing to zero at 6.6% strain. Beyond this level of strain, cohesion continues to decrease to negative values, possibly due to the effects of matric suction. Deviator stress-strain curves are also presented in Figure 6.7.

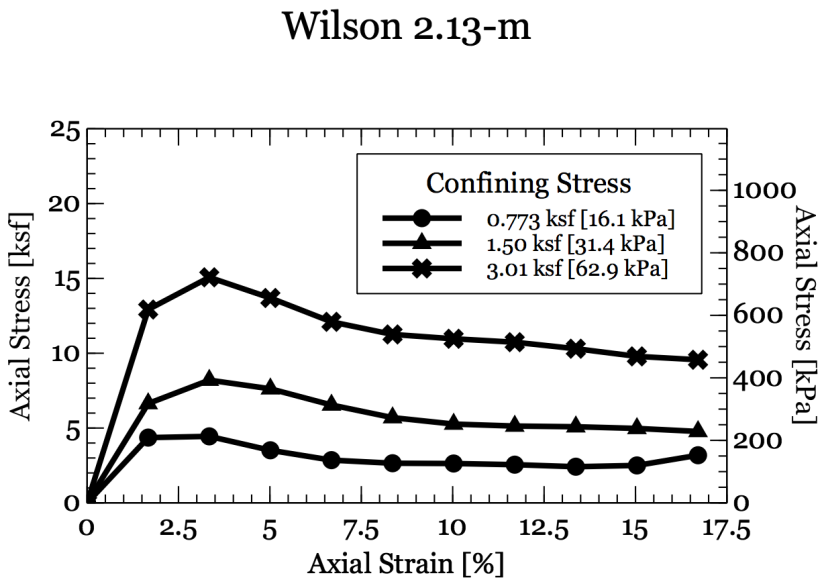

Figure 6.7: Triaxial stress-strain curves for Wilson 2.13-m wall

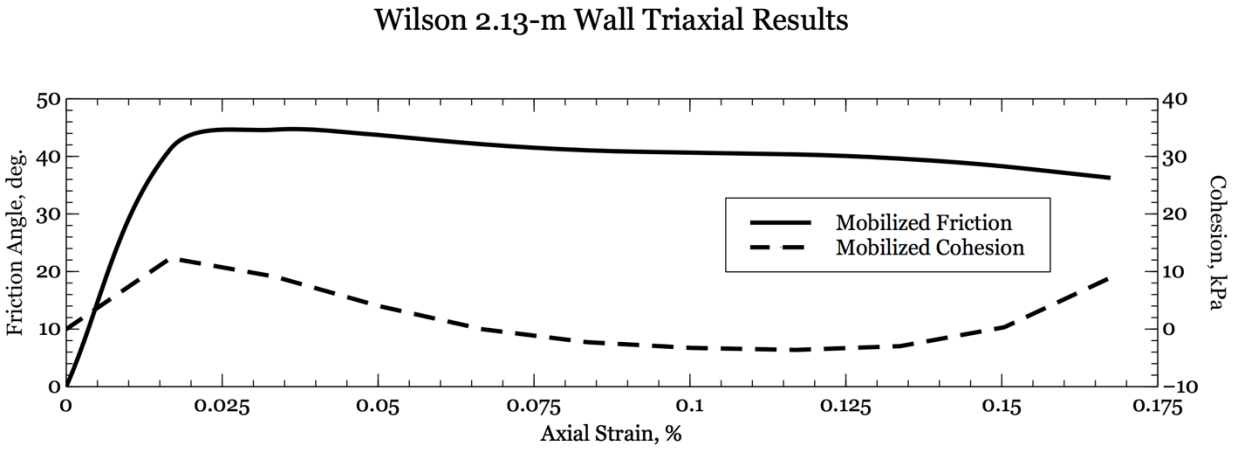

Figure 6.8: Mobilized friction angle and cohesion for Wilson 2.13-m wall

Based on the back-calculations reported by Wilson, wall soil friction was taken as 3 degrees. Compressive stiffness values were estimated based on the deviator stress curves and used to evaluate the backfill displacement at each of four stages in the wall loading process. The calculated log-spiral wedge was discretized into 10 slices to evaluate the total

passive strength, while an 18.3-m wide column of backfill (four times the wall length) was also discretized into 10 slices for compression calculations. The results of the analysis are shown below, in Table 6.5, with the resulting passive resistance curve plotted in comparison to the load test results for Test 2 in Figure 6.9. This plot shows peak resistance to be 390 kN/m at a displacement of approximately 5.0 cm.

Table 6.3: Model results for Wilson 2.13-m wall test

Stage	ε_a	Φ'_m *(deg)*	C'_m *(kPa)*	∂' *(deg)*	P_p *(kN/m)*	M *(m²/kN)*	Δ *(cm)*
(0)	(0)	(0)	(0)	(0)	(0)	(0)	(0)
1	1.7%	41.3	12.3	3	367	1.78E-4	3.2
2	3.3%	29.8	9.1	3	383	3.49E-4	6.6
3	6.7%	42.1	0	3	240	1.08E-3	13.0
4	11.7%	40.3	3.6	3	184	2.13E-3	19.6

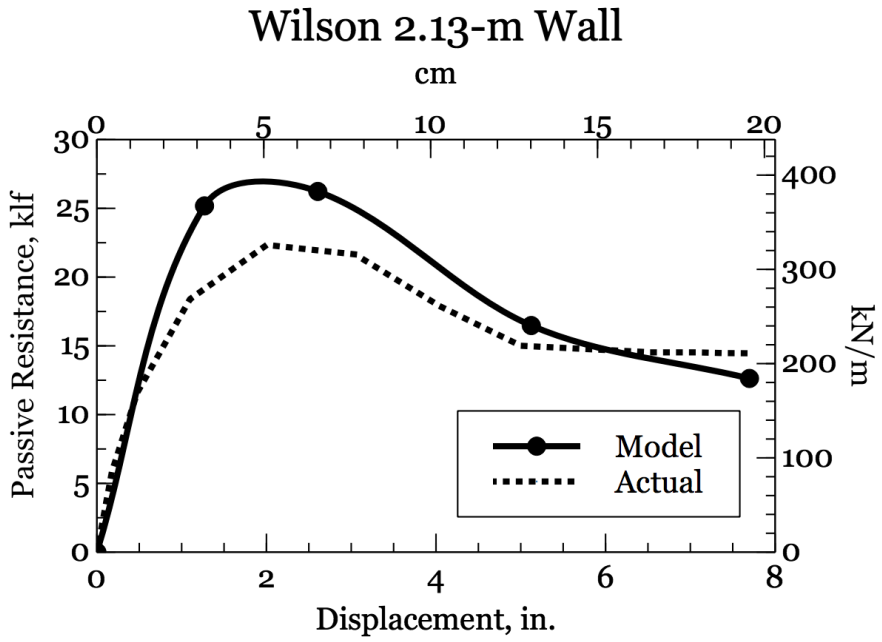

Figure 6.9: Load-deflection curves (model and experimental) for Wilson 2.13-m wall

7 DISCUSSION

Comparative Results

Table 7.1 presents results from each case study, with analytical results reported opposite experimental results for each case study, along with results using the methods published by Duncan and Mokwa (2001) and Shamsabadi (2007).

Table 7.1: Result comparisons for each abutment wall test case

	Lemnitzer 1.68-m			*Lemnitzer 2.44-m*			*Wilson 2.13-m*		
	Experimental	*Proposed*	*LSH*	*Experimental*	*Proposed*	*LSH*	*Experimental*	*Proposed*	*LSH*
K_{50} *(kN/cm/m)*	*317*	*147*	*290*	*145*	*149*	*270*	*140*	*141*	*150*
$P_{p,\,max}$ *(kN/m)*	*484*	*423*	*443*	*707*	*768*	*545*	*326*	*390*	*315*
$K_{p,\,max}$	*16.3*	*14.9*	*15.8*	*11.9*	*12.7*	*13*	*6.82*	*816*	*6.59*
y_{max} *(cm)*	*4.98*	*3.89*	*8.35*	*12.0*	*17.2*	*24.4*	*5.08*	*5*	*5*

Model Accuracy

Based on the data in Table 7.1, the proposed method reasonably predicts both the passive capacity, and the displacement required to induce the passive capacity. However, the proposed method less consistently predicts the 50% loading stiffness (K_{50}) relative to other methods shown here. This is likely due to the fact that the analytical output is directly

provided from the conditions of the sample being tested. While "seating" pressures from the triaxial load actuator are intended to approximate at-rest conditions in the wall backfill prior to passive loading, in actuality there is often insufficient control over this portion of the testing process. This may result in the discrepancies in the K_{50} values.

Further, while the proposed method captures the shape of the load-deflection curve (a feature shared only with computer-based finite element/difference analysis methods), there is noticeable variability in the error at each analysis point. While this could be the result of experimental error transmitted from the laboratory testing throughout the analysis, the high sensitivity of the method of slices to interslice shear suggests that assumptions regarding the wall friction development and propagation through the soil mass may be a contributing factor. Each of the three case studies applied a different wall friction model in their respective analyses. Given that wall friction was measured in the 1.68-m test, its corresponding analytical model applied a wall friction bilinear model to approximate the experimental observations, linearly decreasing from $\partial_m = \phi'_m = 16.4°$ at a displacement of 1.93 cm to $\partial_m = 15°$ at a displacement of 4.01 cm (and maintaining 15° thereafter). The 2.44-m wall test analysis applied interslice shear angles equal to $\partial_m = \phi'_m = 11.3°$ at a displacement of 1.94 cm to $\partial_m = 18°$ at a displacement of 12.5 cm (and maintaining 18° thereafter). The 2.13-m test analysis used a static wall friction angle of 3° as reported by Wilson et al.

Advantages of Proposed Method

The advantages of analytical modeling of wall performance based on laboratory test performance are readily understood: primarily, that one might not need to load-test an

abutment wall to obtain data on its strength under passive loading. Analytical models inform the design of such structures prior to and during the design process, allowing for the construction of efficient, safe, and serviceable walls. This proposed method has the distinct advantage over other methods in that (a) laboratory test data *directly* informs the analysis; (b) the analysis is not limited to contractive, strain-hardening behavior modeling; and (c) the evaluation does not require complex, specialized software to perform, and may be conducted using typical spreadsheet software. Given these properties, the analyst is offered a great deal of flexibility in their evaluation of passive resistance; sensitivity and "what if"-type analyses are comparatively simple and expedient as when performed using common geotechnical FEA software. Further, the fact that the analytical results are direct mechanical evaluations of experimental test values shifts the emphasis away from empirical correlations and scaling factors, and shows good faith in uncovering a more mechanistic understanding of the mobilized passive behavior of abutment walls. The general agreement of the analytical and experimental results of the case studies herein shows the robust potential of the proposed method.

Limitations and Drawbacks of Proposed Method

The primary limitation of the proposed procedure is the simplicity of the model used to predict displacement. For example, only maximum principal strains are considered with regard to displacement evaluation; axial and shear strains are not analyzed as separate components. This is in conflict with the natural understanding that both, shear and axial strains, contribute differently to the total displacement behavior, especially as the angle of the failure plane changes along its length.. However, independent measurement of

each strain parameter is a luxury not often provided (or depending on the laboratory setup, possible) in laboratory shear testing. As such, while simplified mechanical assumptions are made in the evaluation of the proposed model, these only facilitate realistic inputs from triaxial test results.

Another fundamental shortcoming with the proposed method is the set of assumptions included as a part of the soil strength and displacement models. One of these is the assumption that wall friction dissipates into the backfill, decreasing linearly further from the wall face, reaching zero as the curved failure wedge transitions to the Rankine wedge. This stress propagation model is taken directly from Terzaghi's 1948 work on earth pressures, with little advancement in theory or understanding in the time since, based on the author's research. The development of a more accurate theory of the influence of wall friction would require detailed load test measurements, including stresses and strains at regular intervals in the backfill area as well as at the wall/soil interface. To date, most load tests have focused primarily on measuring reaction forces on the wall by the soil, and measurement of the failure plane geometry, which does not provide enough data for any more detailed analysis of stress or strain propagation than what is presented herein.

One characteristic particular to analytical models based directly on laboratory test data is that the results may be specifically related to the testing conditions of the soil sample--such as moisture content, density consistency, drained/undrained conditions. While some of these conditions may be categorically assumed (for example, a clayey backfill may be assumed to fail in an undrained state for relatively rapid loading conditions), some of these properties may vary in the design wall system depending on elapsed time, weather conditions, etc. One such case occurred in the Wilson load tests,

where data from the triaxial tests proved to model load test 2 much more closely than load test 1. The author posited that the load test discrepancy occurred due to variations in the shear strength profile of the soil as the result of differences in moisture content; given that load test 2 rested for less time before loading (3 days as opposed to 20 days for test 1), its in situ condition better matched the conditions of the triaxial sample as conducted herein. As such, predicted wall performance is highly contingent on triaxial testing conditions, which should be chosen carefully to evaluate the anticipated critical conditions of an abutment wall system.

8 SUMMARY AND RECOMMENDATIONS

Current design practice for retaining walls often involves analysis of passive resistance development with respect to wall mobilization, but often consists only of comparison with a generalized graphical relationship as shown in Figure 2.6. While Duncan and Mokwa (2001) and Shamsabadi, etal. (2005, 2007, 2009) provided analytical solutions for the predictive load-deflection modeling of simple retaining structures under passive conditions, these models rely on empirically-derived correlations, and only accurately capture hyperbolically-shaped load deflection curves. Analytical methods that implement direct soil strengths and behavioral data and account for different load-deflection relationship shapes would be potentially more intuitive and pertinent for implementation in geo-structural analysis and design.

As described in this document, a passive load-deflection model was devised, employing direct shear strength mobilization data, a log-spiral passive wedge configuration, and horizontal backfill compression analysis through influence factor evaluation. Three case studies of experimental wall load tests were analyzed using this method, with results in reasonable agreement with both the actual performance of the load tests and the load-deflection curve shape. Since influence-factor based soil displacement analysis is commonplace in geotechnical engineering, the inclusion of mobilized shear parameter evaluation yields a valuable, applicable tool for modelling load-deflection behavior of simple retaining walls.

Given the sensitivity of direct mechanical analysis of earth structures to laboratory soil test data, future research should involve comparative analysis of experimental load tests to multiple variations of testing procedures—perhaps even direct shear testing—in

order to provide a more definitive commentary on strength parameters over a variety of backfill types and wall configurations. This would involve the collection, cataloguing, and analysis of a large number of wall tests, so that trends could be established based upon multiple unique load tests for each respective wall configuration, backfill soil type, load rate, etc. Of specific interest is the disparity in the Wilson et al. (2010) experimental results, wherein wall performance was apparently directly related to the time between construction and testing. While the current state of research using mobilized passive resistance intends to accurately model in-situ conditions, design practice often involves analysis of the most critical configurations that could occur in the field (e.g., evaluation of performance at the poorest allowable quality control, unfavorable moisture conditions, etc.). While one might assume which parameters will reduce wall performance when altered, it is often too costly or intensive to perform multiple suites of laboratory testing and subsequent analysis to provide an expected wall load-deflection relationship as well as a design-critical one. Developing an envelope-based procedure for simple retaining walls would be valuable to account for the various loading conditions and scenarios checked in the design process.

Lastly, further studies should be performed regarding how wall friction mobilizes and propagates throughout wall backfills undergoing passive loading, specifically as it relates to soil-to-soil mobilized shear strength. This would involve experimental load testing of simple retaining walls with a three-dimensional matrix of instruments in the backfill to measure stresses as the wall begins to displace and passive resistance begins to develop. Given the high sensitivity of calculated passive resistance to wall friction, further

understanding of how interslice friction propagates will reduce error in the predicted load-deflection curves.

9 REFERENCES

Amsiejus, Jonas, Dirgeliene, Neringa, & Norkus, Arnoldas. (2010). Analysis of Methods for Evaluation of Soil Shear Strength Parameters. *10th International Conference "Modern Building Materials, Structures and Techniques", Vol. 2.* 1077-1082.

Baishya, Sukumar. (2012). Evaluation of Seismic Active Earth Pressure Using Horizontal Slice Method and Log-Spiral Failure Surface. *15th World Conference on Earthquake Engineering (15WCEE)*.

Bozorgzadeh, A., Ashford, S. A., Restrepo, J. I., & Nimityongskul, N. (2008). Experimental and Analytical Investigation on Stiffness and Ultimate Capacity of Bridge Abutments, (59).

Brinkgreve, R.B.J., Engin, E., & Swolfs, W.M. (2014). "PLAXIS 2014 material models manual". Rotterdam, Netherlands.

Chen, W. F., & Scawthorn, C. R. (1970). Limit Analysis and Limit Equilibrium Solutions in Soil Mechanics. *Soils and Foundations*, *10*(3), 13–49. https://doi.org/10.3208/sandf1960.10.3_13

Chugh, A. K. (1995). A Unified Procedure for Earth Pressure Calculations.

Civil and Structural Engineer Magazine. (2014). "Lessons in Large Retaining Walls." Retrieved from https://csengineermag.com/article/lessons-in-large-retaining-walls/

Duncan, J. M., & Mokwa, R. L. (2001). Passive Earth Pressures: Theories and Tests. *Journal of Geotechnical and Geoenvironmental Engineering*, *127*(3), 248–257. https://doi.org/10.1061/(ASCE)1090-0241(2001)127:3(248)

Fang, Y.-S., Ho, Y.-C., & Chen, T.-J. (2002). Passive Earth Pressure with Critical State Concept. *Journal of Geotechnical and Geoenvironmental Engineering*, *128*(October), 651–659. https://doi.org/10.1061/(ASCE)1090-0241(2002)128:8(651)

Hussey, D. E. (1995). Competence Based Competition. *Journal of Strategic Change*, *4*, 181–182. Retrieved from http://search.ebscohost.com/login.aspx?direct=true&db=bth&AN=17391750&site=ehost-live

Itasca Consulting Group. (2018). "FLAC Version 8.0". Retrieved December 19, 2018, from https://www.itascacg.com/software/flac

José Medina, Nicolás Sau, & Jesús Quintana. (2016). Lateral Displacement of Retaining Walls. *Journal of Geological Resource and Engineering*, *4*(6), 251–256. https://doi.org/10.17265/2328-2193/2016.06.001

Lemnitzer, A., Ahlberg, E. R., Nigbor, R. L., Shamsabadi, A., Wallace, J. W., & Stewart, J. P. (2009). Lateral Performance of Full-Scale Bridge Abutment Wall with Granular Backfill. *Journal of Geotechnical and Geoenvironmental Engineering*. https://doi.org/10.1061/(ASCE)1090-0241(2009)135:4(506)

Lemnitzer, A., Hilson, C., Nojoumi, A., Taciroglu, E., Wallace, J. W., & Stewart, J. P. (2012). Experimental Assessment of the Passive Resistance of a Bridge Abutment System with Various Backfill Heights. *GeoCongress 2012*, 2088–2097. https://doi.org/10.1061/9780784412121.214

Sarath Chandra Reddy, N., Dewaikar, D. M., & Mohapatro, G. (2014). Computation of passive pressure coefficients: for a horizontal cohesionless backfill with surcharge using method of slices. *International Journal of Geotechnical Engineering*, *8*(4), 463–468. https://doi.org/10.1179/1939787913Y.0000000037

Sarath, N., Reddy, C., Dewaikar, D. M., & Mohapatra, G. (2013). Computation of Passive Earth Pressure Coefficients for a Horizontal Cohesionless Backfill Using the Method of Slices. *Cloud Publications International Journal of Advanced Civil Engineering and Architecture Research*, *2*(1), 32–41. https://doi.org/10.1179/1939787913Y.0000000037

Schmertmann, J. H. (2012). New concepts for the mobilization of the components of shear resistance in clay. *Norwegian Geotechnical Institute*. https://doi.org/10.1016/j.cmet.2006.04.011

Sekkel, A., & Meghachou, M. (2013). The Effect of Displacement Mode of Rigid Retaining Walls on Shearing Bands by Active Earth Pressure. *ETASR - Engineering, Technology & Applied Science Research*, *3*, 526–531.

Shamsabadi, A., Ashour, M., & Norris, G. (2005). Bridge Abutment Nonlinear Force-Displacement-Capacity Prediction for Seismic Design. *Journal of Geotechnical and Geoenvironmental Engineering*, *131*(2), 151–161. https://doi.org/10.1061/(ASCE)1090-0241(2005)131:2(151)

Shamsabadi, A., Rollins, K. M., & Kapuskar, M. (2007). Nonlinear Soil–Abutment–Bridge Structure Interaction for Seismic Performance-Based Design. *Journal of Geotechnical and Geoenvironmental Engineering*, *133*(6), 707–720. https://doi.org/10.1061/(ASCE)1090-0241(2007)133:6(707)

Terzaghi, K. (1941). General wedge theory of earth pressure. *American Society of Civil Engineers Transactions*. https://doi.org/10.1089/jwh.2006.15.763

Terzaghi, K., & Peck, R. B. (1948). Soil Mechanics in Engineering PracticeWiley. *New York*. https://doi.org/10.1016/S0013-7952(97)81919-9

Vistazo, E. (2016). *Volumen 3*.

Wilson, P., & Elgamal, A. (2010). Large-Scale Passive Earth Pressure Load-Displacement Tests and Numerical Simulation. *Journal of Geotechnical and Geoenvironmental Engineering*, *136*(12), 1634–1643. https://doi.org/10.1061/(ASCE)GT.1943-5606.0000386